

# Quantum optical analysis of high-harmonic generation in solids within a Wannier-Bloch picture

J. Rivera-Dean,<sup>1,\*</sup> P. Stammer,<sup>1</sup> A. S. Maxwell,<sup>2</sup> Th. Lamprou,<sup>3,4</sup> A. F.

Ordóñez,<sup>1</sup> E. Pisanty,<sup>5</sup> P. Tzallas,<sup>3,6</sup> M. Lewenstein,<sup>1,7</sup> and M. F. Ciappina<sup>8,9,10,†</sup>

<sup>1</sup>*ICFO – Institut de Ciències Fotoniques, The Barcelona Institute of Science and Technology, 08860 Castelldefels (Barcelona)*

<sup>2</sup>*Department of Physics and Astronomy, Aarhus University, DK-8000 Aarhus C, Denmark*

<sup>3</sup>*Foundation for Research and Technology-Hellas,*

*Institute of Electronic Structure & Laser, GR-70013 Heraklion (Crete), Greece*

<sup>4</sup>*Department of Physics, University of Crete, P.O. Box 2208, GR-70013 Heraklion (Crete), Greece*

<sup>5</sup>*Department of Physics, King's College London, WC2R 2LS London, United Kingdom*

<sup>6</sup>*ELI-ALPS, ELI-Hu Non-Profit Ltd., Dugonics tér 13, H-6720 Szeged, Hungary*

<sup>7</sup>*ICREA, Pg. Lluís Companys 23, 08010 Barcelona, Spain*

<sup>8</sup>*Physics Program, Guangdong Technion–Israel Institute of Technology, Shantou, Guangdong 515063, China*

<sup>9</sup>*Technion – Israel Institute of Technology, Haifa, 32000, Israel*

<sup>10</sup>*Guangdong Provincial Key Laboratory of Materials and Technologies for Energy Conversion,*

*Guangdong Technion – Israel Institute of Technology, Shantou, Guangdong 515063, China*

(Dated: November 2, 2022)

The quantum optical characterization of strongly laser-driven matter interactions may allow to extend current quantum technology platforms to unprecedented time and energy scales. In this work, we make a step forward in this direction by studying high-harmonic generation processes in solid-state systems under a quantum optical framework. We do this under a Wannier-Bloch approach, which allows us to perform a direct comparison with the analysis that has been already done for gaseous systems. This allows us to study the photon number probability distribution of the light obtained after emission, and relate its features with those found in usual HHG spectra. Furthermore, after performing the corresponding quantum operations that allow us to restrict ourselves to HHG processes, we find an entangled state between the field modes and the different Wannier states where the electron can be found after recombination, but also between the field modes themselves. We study the non-classical features of this state, and quantify the light-matter entanglement and the entanglement between the field modes.

## I. INTRODUCTION

High-harmonic generation (HHG) is one of the most studied processes within the field of strong laser-matter interactions [1], and has found numerous applications in attosecond science [2–4], nonlinear XUV optics [5–12] and high-resolution spectroscopy [13, 14], among others. In general terms, HHG consists of the generation of high-frequency radiation resulting from the interaction of an intense femtosecond laser source with matter. This radiation is typically emitted as a periodic series of ultrashort attosecond bursts of radiation, which combine to form a comb of harmonics of the driving laser that spans dozens, hundreds or even thousands of harmonic orders [15].

Within the context of atoms, the physics behind this process are resumed in the so-called three-step model [16–19], according to which an electron (i) is ripped away from the atom, (ii) accelerates in the continuum driven by the field, and (iii) recollides with the parent ion liberating the gained kinetic energy in form of high-frequency radiation. For solid-state systems [2, 20–22], the process underlying the generation of harmonic radiation becomes more complex [23, 24], as the atoms are more

densely packed and their electrons interact strongly with their surroundings. Thus, on top of the transitions between the valence and conduction bands (interband transitions), which find their analogy in gaseous HHG with the ionization and recombination steps, in solid-state media the electron can also undergo excitations within the same band (intraband transitions). This is a crucial difference, as it increases the delocalization of the electron, allowing it to recombine, in the emission step later on, with a different state from the one in which it had initially started the dynamics. Because of this, the resulting HHG spectrum differs in some aspects with respect to its gaseous counterpart, such as a weaker dependence of the harmonic emission on the field's ellipticity [23, 25, 26] or a different scaling of the cutoff frequency with the driving electric field amplitude [16, 25].

In this work, we provide a quantum optical description of the light-matter interaction between a solid-state system and a the quantized electromagnetic field. From the usual semiclassical perspective, under which the solid system is treated quantum mechanically while the field classically, many approaches have been proposed to model the harmonic emission [23, 24, 27–50]. Of particular interest for the description we provide here, is the model employed in Ref. [27] where the solid system is described under a mixed representation, such that Wannier states are used for describing the valence band and Bloch states

---

\* [javier.rivera@icfo.eu](mailto:javier.rivera@icfo.eu)

† [marcelo.ciappina@gtiit.edu.cn](mailto:marcelo.ciappina@gtiit.edu.cn)

are used for the conduction band. Because Wannier states are *spatially localized* [51], this picture allows to establish a much more transparent analogy with the atomic picture, while predicting similar HHG spectra to the outcome of other models where both valence and conduction band are depicted under a Bloch-Bloch approach [23]. On the other hand, from a quantum optical perspective, strong-field processes have been studied experimentally and theoretically, so far, only for atomic ensembles [52–63]. These works have shown that, strong laser-matter interaction processes can lead to the generation of high-photon number non-classical states of light [55, 58, 62], where the generated harmonics are entangled between them [61, 62, 64] and with the electron that gets ionized [60]. Thus, it is of interest to understand to what extent the features that are observed in the atomic regime can be found in the solid-state scenario. With that purpose in mind, in this work we apply the conditioning operations that allow for the generation of non-classical states of light in gaseous HHG [55, 58, 61, 64] to its solid-state counterpart, and study the properties of the obtained state.

The article is organized as follows. In Section II we present the theoretical analysis, where we introduce the Hamiltonian governing the system dynamics, and study the corresponding Schrödinger equation analytically by implementing some transformations and approximations. In Section III we present the results, which are divided into three subsections. Firstly, we study how the dynamics of the electron in the valence and conduction bands affect the quantum optical state of the system; secondly, we focus on the high-harmonic generation processes, and study the photon number probability of finding a harmonic photon in one of the field modes; thirdly, we introduce the *conditioning to HHG* operation as experimentally implemented in [58, 65], and theoretically described in [61, 62, 64], to study non-classical properties of the obtained quantum state. Finally, we end our contribution with conclusions and a brief outlook in Section IV, where we also discuss how decoherence effects in solid-state systems may affect the measured quantum optical observables.

## II. THEORETICAL ANALYSIS

In typical experimental realizations of intense laser-matter interactions with solid-state systems, the applied laser field hits the target perpendicularly and generates the harmonic radiation along the transmission path [25, 66]. The wavelength of the applied laser field in these scenarios usually belongs to the mid-infrared (MIR) regime ( $\lambda \sim 3 - 8 \mu\text{m}$ ), which is much larger than the typical lattice constant  $a$  ( $\sim 1 \text{\AA}$ ). Thus, within the present analysis, we work under the dipole approximation and the single active electron (SAE) approximation [67], such that the Hamiltonian describing the interaction of

the solid system with the applied field is given by

$$\hat{H} = \hat{H}_{\text{cr}} + e\hat{\mathbf{X}} \cdot \hat{\mathbf{E}} + \hat{H}_{\text{f}}, \quad (1)$$

where we have considered for simplicity a one dimensional model, which restricts us to linearly polarized fields. In this expression,  $\hat{H}_{\text{cr}}$  represents the crystal Hamiltonian and, to characterize it, we consider a two-band model under the tight-binding approximation, and describe the energy dispersion relations for the valence and conduction bands as [68]

$$\begin{aligned} \mathcal{E}_v(k) &= -2I_v \cos(ka), \\ \mathcal{E}_c(k) &= \mathcal{E}'_c - 2I_c \cos(ka), \end{aligned} \quad (2)$$

where  $k$  is the crystal momentum,  $I_v < 0$  and  $I_c > 0$  are the hopping parameters in the valence and conduction bands, respectively, and  $\mathcal{E}'_c = \mathcal{E}_g + 2I_c - 2I_v$  with  $\mathcal{E}_g$  the band-gap energy.

In Eq. (1), we describe the light-matter interaction within the *length gauge* form and under a quantum optical framework [62], in which the electric field is given in terms of

$$\hat{E} = -i \sum_{\mathbf{k},\mu} \sqrt{\frac{\hbar c |\mathbf{k}|}{2\epsilon_0 V}} (\hat{a}_{\mathbf{k},\mu}^\dagger - \hat{a}_{\mathbf{k},\mu}), \quad (3)$$

where  $\hat{a}_{\mathbf{k},\mu}^\dagger$  ( $\hat{a}_{\mathbf{k},\mu}$ ) is the creation (annihilation) operator acting over the mode with wavevector  $\mathbf{k}$  and polarization  $\mu$ ,  $V$  is the quantization volume,  $c$  the speed of light and  $\epsilon_0$  the vacuum permittivity. Finally,  $\hat{H}_{\text{f}}$  represents the free-field Hamiltonian

$$\hat{H}_{\text{f}} = \sum_{\mathbf{k},\mu} \hbar \omega \hat{a}_{\mathbf{k},\mu}^\dagger \hat{a}_{\mathbf{k},\mu}. \quad (4)$$

Similarly to Ref. [27], in this work we study the solid-state system within a mixed representation, where we describe the valence band with a Wannier state representation ( $\{|w_{v,j}\rangle\}$ ) and the conduction band with a Bloch state representation ( $\{|\phi_{c,k}\rangle\}$ ) (see Appendix A for more details about these states). Since the Wannier wavefunctions are *spatially localized* while Bloch wavefunctions are not [51], this framework allows us to recover a similar picture to that of strong laser-matter interactions in atomic systems [3, 19]. Thus, although the initial state of the system corresponds to a completely filled Fermi sea, at the level of single-electron dynamics we consider the initial state of our Schrödinger equation to be

$$|\Psi(t_0)\rangle = |w_{v,j_0}\rangle \bigotimes_{\mathbf{k} \in \text{IR}} |\alpha_{\mathbf{k}}\rangle \bigotimes_{\mathbf{k} \in \text{HH}} |0_{\mathbf{k}}\rangle, \quad (5)$$

that is, the electron is initially placed in the Wannier site  $j_0$  of the valence band, the photonic modes that belong to the spectrum of the incident laser field ( $\mathbf{k} \in \text{IR}$ ) are in a coherent state of amplitude  $\alpha_{\mathbf{k}}$ , while all the other photonic modes ( $\mathbf{k} \in \text{HH}$ ), that could potentially be excited during the HHG process, lie in a vacuum state  $|0\rangle_{\mathbf{k}}$ .

We note that, although we have selected site  $j_0$  for the electron, all Wannier states are equivalent so one could set  $j_0 = 0$  without loss of generality. As in experimental implementations [25, 66] and other theoretical studies [27, 36], we restrict to field amplitudes that are lower than the damage threshold of the material ( $|\alpha| \propto 10^5 - 10^6$ ,  $I_0 \propto 10^{10} \sim 10^{11}$  W/cm<sup>2</sup> with  $I_0$  the peak intensity of the driving pulse).

The Schrödinger equation characterizing the dynamics of our system results

$$i\hbar \frac{\partial |\Psi(t)\rangle}{\partial t} = (\hat{H}_{\text{cr}} + e\hat{X} \cdot \hat{E} + \hat{H}_{\text{f}}) |\Psi(t)\rangle. \quad (6)$$

In order to solve this equation, we first simplify it by applying some unitary operations. Specifically, we: (i) move to the interaction picture with respect to the free-field term  $\hat{H}_{\text{f}}$  so that the electric field operator becomes time-dependent,

$$\hat{E}(t) = -i \sum_{\mathbf{k},\mu} \sqrt{\frac{\hbar c |\mathbf{k}|}{2\varepsilon_0 V}} (\hat{a}_{\mathbf{k},\mu}^\dagger e^{i\omega_{\mathbf{k}} t} - \hat{a}_{\mathbf{k},\mu} e^{-i\omega_{\mathbf{k}} t}), \quad (7)$$

and (ii) work in a displaced frame with respect to the driving field, such that the electric field operator splits into a *classical* term  $E_{\text{cl}}(t)$ , which depicts the expectation value of the field

$$E_{\text{cl}}(t) = -i \sum_{\mathbf{k}} \sqrt{\frac{\hbar c |\mathbf{k}|}{2\varepsilon_0 V}} (\alpha_{\mathbf{k}}^* e^{i\omega_{\mathbf{k}} t} - \alpha_{\mathbf{k}} e^{-i\omega_{\mathbf{k}} t}), \quad (8)$$

and another term  $\hat{E}(t)$ , with the same form as the one shown in Eq. (7), that represents the quantum optical fluctuations around the mean value. Furthermore, within this frame of reference, the initial state of our system is given by  $|\Psi'(t_0)\rangle = |w_{v,j_0}\rangle \otimes_{\mathbf{k}} |0_{\mathbf{k}}\rangle$ , and the corresponding Schrödinger equation by

$$i\hbar \frac{\partial |\Psi'(t)\rangle}{\partial t} = (\hat{H}_{\text{cr}} + e\hat{X} E_{\text{cl}}(t) + e\hat{X} \hat{E}(t)) |\Psi'(t)\rangle, \quad (9)$$

where  $|\Psi'(t)\rangle = \prod_{\mathbf{k} \in \text{IR}} D(\alpha_{\mathbf{k}}) e^{-\frac{i}{\hbar} H_{\text{f}} t} |\Psi(t)\rangle$ .

With the aim of solving the Schrödinger equation above, we decompose the state by means of a mixed representation of the electronic degrees of freedom

$$|\Psi'(t)\rangle = \sum_j a_j(t) |w_{v,j}\rangle |\Phi_{v,j}(t)\rangle + \int_{\text{BZ}} dk a_c(k,t) |\phi_{c,k}\rangle |\Phi_c(k,t)\rangle, \quad (10)$$

where the first term represents the case where the electron interacts with the field but ends up in a Wannier state  $|w_{v,j}\rangle$  of the valence band, while the second term represents an excitation of the electron to a Bloch state  $|\phi_{c,k}\rangle$  of the conduction band. In this decomposition, and unlike the one presented in [27], every contribution is multiplied by a quantum optical component ( $|\Phi_{v,j}(t)\rangle$

and  $|\Phi_c(k,t)\rangle$  respectively) that describes the state in which the quantum optical field lies after each of the possible events. Note that this is the most general hypothesis one can consider for the interaction of a driving field with a two-band solid-state model.

Under this mixed representation, the matrix elements of the crystal Hamiltonian,  $\hat{H}_{\text{cr}}$  are given by

$$\langle w_{v,j} | \hat{H}_{\text{cr}} | w_{v,j} \rangle = -I_v \delta_{|j-j'|,1}, \quad (11)$$

$$\langle \phi_{c,k} | \hat{H}_{\text{cr}} | \phi_{c,k'} \rangle = \mathcal{E}_c(k) \delta(k - k'), \quad (12)$$

where in Eq. (11) we have considered that the electron can only hop to its nearest-neighbor sites, although one could generalize this model by introducing hopping terms to other sites. On the other hand, for the transition matrix elements we have (see Appendix A for a detailed derivation)

$$\langle \phi_{c,k} | \hat{X} | \phi_{c,k'} \rangle = i\hbar \frac{\partial}{\partial k} \delta(k - k'), \quad (13)$$

$$e \langle \phi_{c,k} | \hat{X} | w_{v,j} \rangle = \tilde{w}_v^* e^{ikx_j} d_{v,c}(k), \quad (14)$$

$$\langle w_{v,j} | \hat{X} | w_{v,j'} \rangle = x_j \delta_{j,j'}. \quad (15)$$

In Eq. (14) we have that  $\tilde{w}_v$  is a normalization constant, which in the case of one dimensional systems is independent of the crystal momentum [69]. On the other hand, we have that  $d_{v,c}(k) = \langle \phi_{v,k} | \hat{X} | \phi_{c,k} \rangle$ . The values that this quantity can acquire are tabulated and can be found in the literature (see for instance Refs. [70–73]).

## A. Conduction band analysis

Firstly, we proceed to study the dynamics of the electron once it is found in the conduction band. With that aim, we project Eq. (9) by a Bloch state in the conduction band  $|\phi_{c,k}\rangle$  such that, when considering this premise in Eq. (10), the Schrödinger equation reads (for a step-by-step derivation see Appendix B 1)

$$i\hbar \frac{\partial}{\partial t} (a_c(k,t) |\Phi_c(k,t)\rangle) = \mathcal{E}_c(k) a_c(k,t) |\Phi_c(k,t)\rangle + (\hat{E}(t) + E_{\text{cl}}(t)) \sum_j a_j(t) d_{jc}^*(k) |\Phi_{v,j}(t)\rangle + i\hbar e (\hat{E}(t) + E_{\text{cl}}(t)) \frac{\partial}{\partial k} (a_c(k,t) |\Phi_c(k,t)\rangle), \quad (16)$$

where  $d_{jc}(k) = e \langle w_{v,j} | \hat{X} | \phi_{c,k} \rangle$ . The first term at the right hand side of this expression introduces the energy of an electron that is in the conduction band with crystal momentum  $k$ . The second describes an interband transition to the valence band from an electron that finds itself in Wannier site  $j$  of the valence band right before the excitation. Finally, the third one depicts an intraband transition within the conduction band.

In order to solve the differential equation in (16), we consider that the electronic trajectories in the valence

band do not get affected by the quantum optical fluctuations, and are entirely governed by the mean value of the applied field [60]. Moreover, instead of working with the crystal momentum  $k$ , we perform another unitary operation and work with the canonical momentum  $p = k + \frac{e}{c}A(t)$ , where  $A(t)$  is the vector potential of the laser field given by  $E_{\text{cl}}(t) = -(1/c)\partial A(t)/\partial t$ , and which is defined in the *shifted* Brillouin zone  $\text{BZ} = \text{BZ} - A(t)$ . With all the above, and under the initial conditions in Eq. (5), we find (see Appendix B 1)

$$\begin{aligned} a_c(p, t)|\Phi_c(p, t)\rangle &= \frac{1}{i\hbar} \sum_j \int_{t_0}^t dt_1 e^{-\frac{i}{\hbar}S(p, t, t_1)} \hat{\mathbf{D}}(\delta(p, t, t_1)) \\ &\times (\hat{E}(t_1) + E_{\text{cl}}(t_1)) d_{j,c}^*(p - \frac{e}{c}A(t_1)) \\ &\times a_j(t_1) |\Phi_{v,j}(t_1)\rangle, \end{aligned} \quad (17)$$

where  $S(p, t, t_1)$  is the semiclassical action describing the electron dynamics when propagating from the excitation time  $t_1$  to the final time  $t$ , within the conduction band

$$S(p, t, t_1) = \int_{t_1}^t d\tau \mathcal{E}_c\left(p - \frac{e}{c}A(\tau)\right), \quad (18)$$

and where

$$\hat{\mathbf{D}}(\delta(p, t, t_1)) = \prod_{\mathbf{k}} e^{\varphi_{\mathbf{k}}(p, t_1)} \hat{D}(\delta_{\mathbf{k}}(p, t, t_1)), \quad (19)$$

with  $\hat{D}(\cdot)$  the displacement operator [74, 75]. Thus, similarly to the atomic case [60, 62], during the electron dynamics in the conduction band, the field modes get displaced by an amount  $\delta_{\mathbf{k}}(p, t, t_1)$  given by

$$\delta_{\mathbf{k}}(p, t, t_1) = -\frac{e}{\hbar} \sqrt{\frac{\hbar c |\mathbf{k}|}{2\epsilon_0 V}} \int_{t_1}^t d\tau \Delta r(p, \tau, t_1) e^{i\omega_{\mathbf{k}}\tau}, \quad (20)$$

where  $\Delta r(p, t, t_1)$  is the displacement performed by the electron in the conduction band from time  $t_1$  to  $t$ , i.e.

$$\Delta r(p, t, t_1) = \int_{t_1}^t d\tau \frac{\partial}{\partial p} \left[ \mathcal{E}_v\left(p - \frac{e}{c}A(\tau)\right) \right]. \quad (21)$$

The state in Eq. (17) has a clear interpretation, which is pictorially represented in the upper part of Fig. 1. At time  $t_1$ , the electron finds itself in the Wannier site  $j$  and, at that moment, undergoes an intraband transition mediated by the dipole matrix element  $d_{j,c}^*(p - \frac{e}{c}A(t_1))$ . This interaction is imprinted in the quantum optical degrees of freedom by means of the action of the electric field operator happening at  $t_1$ . Once the electron is in the conduction band, it accelerates until time  $t$ , acquiring a phase  $S(p, t, t_1)$  and, due to its motion, it generates a displacement in the quantum optical degrees of freedom that depends on the specific trajectory that the electron follows during its propagation within the band. Thus, the generated displacement can be understood as an intraband effect that influences the quantum optical state

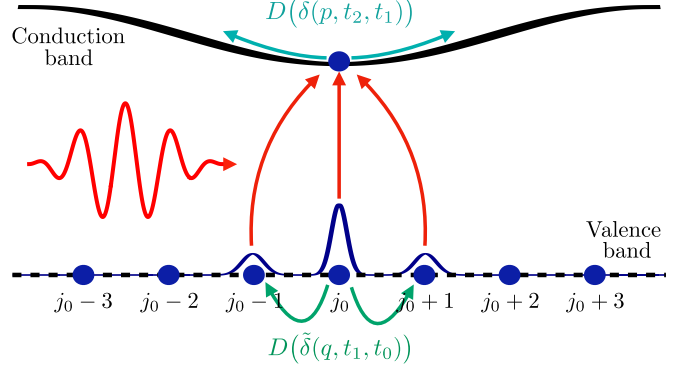


FIG. 1. Pictorial representation of the electron dynamics, and its influence over the displacement generated on the electromagnetic field. When the incident IR field reaches the solid, an electron which is initially in Wannier site  $j_0$  of the valence band, can either perform an interband transition under which it reaches the conduction band, or an intraband transition that populates other neighboring Wannier sites. In the former case, the electron propagates in the conduction band driven by the field, and generates a displacement that affects the field modes which depends on the dynamics within the band. In the latter, the intraband transitions lead to a displacement on the field modes that depends on the dynamics of the electron in the reciprocal space of the valence band.

of the field. We note at this point the similarity of these dynamics with those found for the atomic case after the electron's ionization from the parent system [60, 62]. The main difference between the solid-state case and the latter lies in that the possible values of crystal momentum that the electron can acquire depend on the conduction band's dispersion relation, besides of the laser parameters such as the frequency, duration and electric field amplitude of the applied laser pulse.

## B. Valence band analysis

Thus far, we have studied the effects of the conduction band analysis over the quantum optical state of the field, and presented the similarities with respect to the atomic case. Yet, one of the main differences of the solid-state system with respect to the latter are the many different states from which the electron can reach the conduction band and, eventually, recombine. In most of the atomic system analysis, a single ground state is considered for both ionization and recombination processes and, due to the huge distance between distinct atoms in a gas jet, recombination of electrons belonging to different atoms is highly unlikely. This contrasts with what we find in a solid-state system. In our framework, as there are many different Wannier sites available, an electron could undergo an intraband transition from Wannier site  $j_0$  to  $j'$ , and perform an interband transition to the conduction band from the latter (see lower part of Fig. 1 for a pictorial representation). Moreover, it could potentially

recombine with Wannier site  $j$  that does not necessarily have to be equal to site  $j'$ . Thus, these extra dynamics, which are missing in the atomic picture because of its highly localized nature, lead to additional effects on the quantum optical state of the field.

With the purpose of unveiling the consequences of the valence band dynamics, we project Eq. (9) onto a Wannier state  $|w_{v,j}\rangle$  to get (see Appendix B 2 for a step-by-step derivation)

$$\begin{aligned} i\hbar \frac{\partial}{\partial t} (a_j(t) |\Phi_{v,j}(t)\rangle) = & -I_v a_{j-1}(t) |\Phi_{v,j-1}(t)\rangle - I_v a_{j+1}(t) |\Phi_{v,j+1}(t)\rangle \\ & + (E_{\text{cl}}(t) + \hat{E}(t)) \sum_{j'} d_{j,j'} a_{j'}(t) |\Phi_{v,j'}(t)\rangle \\ & + (E_{\text{cl}}(t) + \hat{E}(t)) \int_{\text{BZ}} dk d_{j,c}(k) a_c(k, t) |\Phi_c(k, t)\rangle, \end{aligned} \quad (22)$$

where  $d_{j,j'} = e\langle w_{v,j} | \hat{X} | w_{v,j'} \rangle$ . In this differential equation, the first two terms at the right hand side introduce the hopping of the electron to its nearest-neighbor sites. On the other hand, and similarly to what we had in the valence band analysis, the other two terms represent, respectively, intraband transitions to other Wannier sites mediated by the electric field, and interband transitions to the conduction band. We note that this last term is proportional to  $eE_0 \sim 10^{-3}$  a.u., with  $E_0$  the field amplitude, which together with the  $a_c(k, t)$  probability amplitude, leads to a term proportional to  $(eE_0)^2$ . Thus, in order to study this equation we consider a perturbative analysis, taking  $(eE_0)^2$  as the perturbation parameter. We then write

$$a_j(t) |\Phi_{v,j}(t)\rangle = a_j^{(0)} |\Phi_{v,j}^{(0)}(t)\rangle + a_j^{(1)} |\Phi_{v,j}^{(1)}(t)\rangle, \quad (23)$$

where the superscript represents the perturbation order. For the zeroth order term we then have to solve

$$\begin{aligned} i\hbar \frac{\partial}{\partial t} (a_j^{(0)}(t) |\Phi_{v,j}^{(0)}(t)\rangle) = & -I_v a_{j-1}^{(0)}(t) |\Phi_{v,j-1}^{(0)}(t)\rangle - I_v a_{j+1}^{(0)}(t) |\Phi_{v,j+1}^{(0)}(t)\rangle \\ & + (E_{\text{cl}}(t) + \hat{E}(t)) \sum_{j'} d_{j,j'} a_{j'}^{(0)}(t) |\Phi_{v,j'}^{(0)}(t)\rangle, \end{aligned} \quad (24)$$

while for the first order term we get

$$\begin{aligned} i\hbar \frac{\partial}{\partial t} (a_j^{(1)}(t) |\Phi_{v,j}^{(1)}(t)\rangle) = & -I_v a_{j-1}^{(1)}(t) |\Phi_{v,j-1}^{(1)}(t)\rangle - I_v a_{j+1}^{(1)}(t) |\Phi_{v,j+1}^{(1)}(t)\rangle \\ & + (E_{\text{cl}}(t) + \hat{E}(t)) \sum_{j'} d_{j,j'} a_{j'}^{(1)}(t) |\Phi_{v,j'}^{(1)}(t)\rangle \\ & + (E_{\text{cl}}(t) + \hat{E}(t)) \int_{\text{BZ}} dk d_{j,c}(k) a_c(k, t) |\Phi_c(k, t)\rangle, \end{aligned} \quad (25)$$

where, in the conduction band term, we consider up to zeroth order terms in  $a_j(t) |\Phi_{v,j}(t)\rangle$ .

We now proceed to solve these two equations separately but, firstly, we introduce some approximations to simplify the analysis. Regarding the relative contribution from interband and intraband transitions to the HHG process, in Ref. [23] it was shown that most of the harmonic emissions comes mainly from interband transitions. However, here we do take into account, at the level of the Schrödinger equation, the full intraband and interband dynamics, as in Ref. [27]. Under these considerations, and after moving to the reciprocal space in the valence band by defining

$$a_q(t) |\Phi_{v,q}(t)\rangle = \sum_j e^{-iqj} a_j(t) |\Phi_{v,j}(t)\rangle, \quad (26)$$

we get that the differential equation for the zeroth order term reads as

$$\begin{aligned} i\hbar \frac{\partial}{\partial t} (a_q^{(0)}(t) |\Phi_{v,q}^{(0)}(t)\rangle) = & -2I_v \cos(q) a_q^{(0)}(t) |\Phi_{v,q}^{(0)}(t)\rangle \\ & + ie\mathbf{a}(\hat{E}(t) + E_{\text{cl}}(t)) \frac{\partial}{\partial q} (a_q^{(0)}(t) |\Phi_{v,q}^{(0)}(t)\rangle), \end{aligned} \quad (27)$$

while for the first order term we have

$$\begin{aligned} i\hbar \frac{\partial}{\partial t} (a_q^{(1)}(t) |\Phi_{v,q}^{(1)}(t)\rangle) = & -2I_v \cos(q) a_q^{(1)}(t) |\Phi_{v,q}^{(1)}(t)\rangle \\ & + ie\mathbf{a}(\hat{E}(t) + E_{\text{cl}}(t)) \frac{\partial}{\partial q} (a_q^{(1)}(t) |\Phi_{v,q}^{(1)}(t)\rangle) \\ & + (\hat{E}(t) + E_{\text{cl}}(t)) \sum_j e^{-iqj} \int_{\text{BZ}} dk d_{j,c}(k) \\ & \times a_c(k, t) |\Phi_c(k, t)\rangle. \end{aligned} \quad (28)$$

We note that these two equations are very similar to that presented in Eq. (16), and can be solved equally under the assumption that the electron trajectories in the valence band are not affected by the quantum optical fluctuations, and by defining  $\tilde{q} = q + \frac{e\mathbf{a}}{\hbar c} A(t)$  (see Appendix B 2 for more details). Hence, we find for the zeroth order term (in real space)

$$\begin{aligned} a_j^{(0)} |\Phi_{v,j}^{(0)}(t)\rangle = & \sum_q e^{iq(j-j_0)} e^{2\frac{i}{\hbar} \tilde{S}(q + \frac{e\mathbf{a}}{\hbar c} A(t), t, t_0)} \\ & \times \hat{\mathbf{D}}(\tilde{\delta}(q + \frac{e\mathbf{a}}{\hbar c} A(t), t, t_0)) \bigotimes_{\mathbf{k}} |0_{\mathbf{k}}\rangle. \end{aligned} \quad (29)$$

The obtained expression has some similarities with that obtained in Eq. (17). Firstly, we observe that, because of the electron dynamics in the reciprocal space of the valence band, we get a phase term that depends on the function  $\tilde{S}(\tilde{q}, t, t_0)$  which is given by

$$\tilde{S}(q, t, t_0) = I_v \int_{t_0}^t d\tau \cos\left(q + \frac{e\mathbf{a}}{\hbar c} A(t) - \frac{e\mathbf{a}}{\hbar c} A(\tau)\right). \quad (30)$$

Secondly, the field modes get affected by a displacement operator in the same way to the one presented in

Eq. (19), but where the generated displacement is now given by

$$\tilde{\delta}_{\mathbf{k}}(\tilde{q}, t) = -2 \frac{e\mathbf{a}}{\hbar} \sqrt{\frac{\hbar c |\mathbf{k}|}{2\epsilon_0 V}} \int_{t_0}^t d\tau \Delta\tilde{r}(\tilde{q}, \tau, t_0) e^{i\omega_{\mathbf{k}}\tau}, \quad (31)$$

where  $\Delta\tilde{r}(\tilde{q}, t, t_0)$  corresponds to the displacement performed by the electron in the reciprocal space of the valence band, and has the form

$$\Delta\tilde{r}(\tilde{q}, t, t_0) = \frac{I_v}{\hbar} \int_{t_0}^t d\tau \sin\left(\tilde{q} - \frac{e\mathbf{a}}{\hbar c} A(\tau)\right). \quad (32)$$

Thus, Eq. (29) describes a process in which the elec-

tron performs an intraband transition to other Wannier sites and, moving through the reciprocal space during this time, induces a displacement in each of the field modes, with this displacement depending on the specific trajectory that it follows in the reciprocal space of the valence band (see Fig. 1). These dynamics could later on continue with a transition to the conduction band, as shown in Eq. (17) and pictorially represented in Fig. 1 with the red arrows that connect the valence and conduction bands.

On the other hand, for the first order term we get the following result

$$\begin{aligned} a_j^{(1)}(t) \left| \Phi_{v,j}^{(1)}(t) \right\rangle &= \sum_{q,j',j''} \int_{t_0}^t dt_2 \int_{BZ} dp \int_{t_0}^{t_2} dt_1 e^{iq(j-j')} e^{2\frac{i}{\hbar}\tilde{S}(q + \frac{e\mathbf{a}}{\hbar c} A(t), t, t_2)} \mathbf{D}(\tilde{\delta}(q + \frac{e\mathbf{a}}{\hbar c} A(t), t, t_2)) (\hat{E}(t_2) + E_{cl}(t_2)) \\ &\times d_{j',c}\left(p - \frac{e}{c} A(t_2)\right) e^{-\frac{i}{\hbar}S(p, t_2, t_1)} \hat{\mathbf{D}}(\delta(p, t_2, t_1)) (\hat{E}(t_1) + E_{cl}(t_1)) d_{j'',c}^*(p - \frac{e}{c} A(t_1)) a_{j''}^{(0)}(t_1) \left| \Phi_{v,j''}^{(0)}(t_1) \right\rangle, \end{aligned} \quad (33)$$

which, on top of the intraband transitions within the valence band from  $t_0$  to  $t_1$ , the interband transition to the conduction band at  $t_1$ , and the electron's propagation together with the associated quantum optical displacement in the field until  $t_2$ , it introduces another extra interaction with the atomic system. Specifically, we observe that at  $t_2$  there is a transition matrix element from the conduction band to Wannier site  $j'$  of the valence band, and consecutive intraband transitions within this band until reaching the final time  $t$ . Thus, the first order term introduces recombination effects and, consequently, describes high-harmonic generation phenomena.

Summing up, when introducing these results in Eq. (10), we can split the resulting state as the sum of three terms, i.e.

$$|\Psi'(t)\rangle = \left| \Psi'^{(0)}(t) \right\rangle + |\Psi'_{\text{ion}}(t)\rangle + |\Psi'_{\text{HHG}}(t)\rangle. \quad (34)$$

The first term in the equation above corresponds to the one shown in Eq. (29), together with the corresponding electronic component, which describes an event where the electron undergoes intraband transitions but never performs an interband transition. The second term identifies with that in Eq. (17) where, on top of the initial intraband transitions, the electron reaches the conduction band but never returns to the valence band. Finally the third one, corresponding to Eq. (33), where the electron undergoes each of the steps of the three-step model, namely performs an interband transition, accelerates within the conduction band and finally returns to the valence band.

### III. RESULTS

This section is divided into three parts. In the first one, we study the displacements  $\delta(p, t, t')$  and  $\tilde{\delta}(\tilde{q}, t, t')$  that are generated due to the electron displacement in the conduction and valence bands, respectively. Afterwards, we focus on the HHG part of the state in Eq. (34), and look at the probability of finding a photon in one of the harmonic modes. Finally, we introduce the so-called *conditioning to HHG* operation that has been theoretically studied and experimentally implemented in Refs. [58, 61, 62, 64, 65], and proceed to characterize the state of the system after such operation.

#### A. Analysis of the photonic displacements in the valence and conduction bands

As mentioned previously, in this section we aim to study the dependence of the photonic displacement due to the electronic motion in the valence and conduction bands. In particular, we consider the cases where the electron moves in the valence band before getting excited, although the results can be extrapolated to the case where the electron propagates in the valence band after the recombination process in HHG.

In Fig. 2, we show the dependence of the displacement with the excitation time. We observe that, for both kind of dynamics, the generated displacement is very small, i.e., in the order of  $|\delta| \sim 10^{-4}$ . In Fig. 2 (a), we show the behavior of the displacement due to the electronic valence band propagation for three different values of  $\tilde{q}$ , while in Fig. 2 (c) we show it for the displacement due

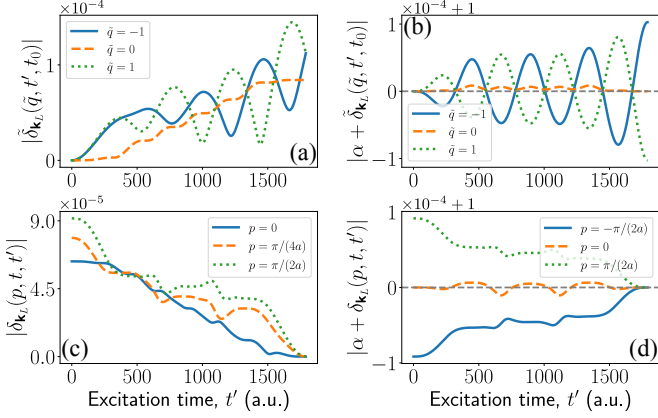


FIG. 2. In (a) and (b) we show the displacement generated due to the motion of the electron within the valence band for different values of  $\tilde{q}$  as a function of the excitation time. In the former, we plot the norm of the displacement, while in latter we show how this displacement affects to the initial coherent state  $\alpha$ , which we set to  $\alpha = 1j$  for representation purposes. Similarly, in (c) and (d) we show the displacement generated due to the motion of the electron within the conduction band for different values of  $p$ . Here, we have used ZnO excited by means of a laser field that has polarization along the  $\Gamma - A$  direction, with 4 cycles of duration, a sinusoidal squared envelope, central wavelength  $\lambda_L = 3.25 \mu\text{m}$ , and peak intensity  $I_0 = 5 \times 10^{11} \text{ W/cm}^2$ .

to the electronic conduction band propagation for three values of  $p$ . For all values of  $\tilde{q}$ , the valence band displacement increases for larger excitation times (via  $t'$ ), while the conduction band displacement is larger for smaller excitation times. This is expected as, the later (sooner) the excitation takes place, the more time the electron spends in the valence (conduction) band, and therefore the more it contributes to the displacement generated on the field. However, there is a key difference with the case of atoms. As shown in Ref. [60], the bigger the final photoelectron momentum, the bigger the final value of the displacement. This is because the electron was able to have arbitrarily big values of momentum, and the generated displacement due to its propagation in the continuum was proportional to  $p$ . However, in this case the energy the electron can have in both the valence and conduction band depends on the cosine of the crystal momentum. Thus, the main consequence this has is that the generated displacement cannot acquire arbitrarily big values by increasing the momentum, as it happens in the case of atoms. This implies that values of  $\tilde{q}$  and  $p$  defined as  $\tilde{q} = \tilde{q}_0 + 2\pi m$  and  $p = p_0 + 2\pi m/a$ , with  $m \in \mathbb{Z}$ , would lead to the same value of the displacement as  $\tilde{q}_0$  and  $p_0$ , respectively. Nevertheless, modifications of  $\tilde{q}$  and  $p$  within the periodicity lead to substantial changes on the generated displacements, as observed in Fig. (2).

Alternatively, one could potentially consider different solid parameters with the aim of increasing the final value of the displacement. As shown in Eq. (32), the displacement in the valence band is directly proportional to the

hopping parameter  $I_v$ . Thus, by considering different solid systems, or excitations along particular solid directions, one could increase or decrease the generated displacement due to the valence band motion. On the other hand, for the displacement due to the motion in the conduction band, the modifications of the solid parameters lead to nontrivial changes, as they already enter at the level of the time-integral (see Eqs. (20) and (21)).

Finally, in Fig. 2 (b) and (d), we show how the different displacements would affect our initial coherent state, which we set here to  $\alpha = 1j$  for representation purposes. We see that both displacements affect differently the initial value of  $\alpha$ . Specifically, for the displacement due to the conduction band motion in Fig. 2 (d) we get a similar behavior as in the atomic case, where positive and negative values of momentum lead to an enhancement and a decreasing, respectively, of the norm  $|\alpha + \delta_{\mathbf{k}_L}(p, t, t')|$  [55, 62]. On the other hand, for the displacement due to the valence band motion in Fig. 2 (b), we observe that there is as well an average phase difference of  $\pi$  for positive and negative values of  $\tilde{q}$ , but with an oscillating behavior that makes the total contribution to increase or decrease the value of  $|\alpha + \tilde{\delta}_{\mathbf{k}_L}(\tilde{q}, t', t_0)|$  at different values of the excitation time.

## B. Probability of finding a photon in the harmonic modes after the HHG process

We now proceed to analyze the HHG part of the state presented in Eq. (34), and study the probability of finding a photon in the harmonic modes. With that purpose, and for the sake of simplicity, we consider hereupon that, whenever the electron undergoes a recombination process and returns to site  $j'$ , it does not propagate to other Wannier sites in the valence band. This allows us to eliminate one of the two terms in the sum appearing in Eq. (33), relaxing the numerical implementation, and allows us to perform a direct comparison with the semiclassical theory presented in Ref. [27]. Furthermore, and taking into account the results obtained in the previous subsection, we consider the effects of the different quantum optical displacements to be negligible, i.e.,  $\tilde{\delta}(\tilde{q}, t_1, t_0) \approx 0$  and  $\delta(p, t_2, t_1) \approx 0$  [76]. Under these assumptions, the HHG part of the state simplifies to

$$\begin{aligned} |\Psi_{\text{HHG}}(t)\rangle \approx & \sum_{j,j'} \int_{t_0}^t dt_2 \int_{\text{BZ}} dp \int_{t_0}^{t_2} dt_1 \\ & \times \hat{E}(t_2) d_{j,c} \left( p - \frac{e}{c} A(t_2) \right) \\ & \times e^{-\frac{i}{\hbar} S(p, t_2, t_1)} \hat{E}(t_1) d_{j',c}^* \left( p - \frac{e}{c} A(t_1) \right) \\ & \times a_{j'}^{(0)}(t_1) |\alpha\rangle \bigotimes_{\mathbf{k} \in \text{HH}} |0_{\mathbf{k}}\rangle |w_{v,j}\rangle. \end{aligned} \quad (35)$$

In order to evaluate this expression, we need to study the effect of the two electric field operators acting at times  $t_1$  and  $t_2$ , onto the initial quantum optical state.

We note that these operators are proportional to  $g(\mathbf{k}) = \sqrt{\hbar c |\mathbf{k}| / (2\epsilon_0 V)}$  which, in our case, is proportional to  $10^{-8}$  (see for instance Ref. [60]). Thus, when evaluating this expression, we keep only those terms that are of first order in  $g(\mathbf{k})$  (see Appendix D). Thus, if we look at the probability of having one photon in one of the harmonic modes, i.e., without considering the fundamental mode, we get

$$P(n_{\mathbf{k}} = 1) = \left| \sum_j \left( \mathcal{P}^{(1)}(j, 1_{\mathbf{k}}, t) + \mathcal{P}^{(2)}(j, 1_{\mathbf{k}}, t) \right) \right|^2, \quad (36)$$

where we have further traced out over all Wannier sites in which the electron can end up. In this expression,  $\mathcal{P}^{(i)}(j, 1_{\mathbf{k}}, t)$  is the probability amplitude of each of the processes that lead to the appearance of an harmonic photon in mode  $\mathbf{k}$ . For one of the processes, which we refer to hereupon as  $i = 1$ , we have the following expression for the probability amplitude

$$\begin{aligned} \mathcal{P}^{(1)}(j, 1_{\mathbf{k}}, t) &= g(\mathbf{k}) \sum_{j'} \int_{t_0}^t dt_2 \int_{\tilde{BZ}} dp \int_{t_0}^{t_2} dt_1 e^{i\omega_{\mathbf{k}} t_2} \\ &\times d_{j,c} \left( p - \frac{e}{c} A(t_2) \right) e^{-\frac{i}{\hbar} S(p, t_2, t_1)} \\ &\times E_{cl}(t_1) d_{j',c}^* \left( p - \frac{e}{c} A(t_1) \right) a_{j'}^{(0)}(t_1), \end{aligned} \quad (37)$$

which we interpret as an excitation event at  $t_1$  of the electron from site  $j'$  in the valence band to the conduction band, and a recombination event at time  $t_2$  where a photon of frequency  $\omega_{\mathbf{k}}$  is generated. Note the analogy of this term with the semiclassical three-step model found in the atomic scenario [19, 77]. On the other hand, for the other process we get

$$\begin{aligned} \mathcal{P}^{(2)}(j, 1_{\mathbf{k}}, t) &= g(\mathbf{k}) \sum_{j'} \int_{t_0}^t dt_2 \int_{\tilde{BZ}} dp \int_{t_0}^{t_2} dt_1 E_{cl}(t_2) \\ &\times d_{j,c} \left( p - \frac{e}{c} A(t_2) \right) e^{-\frac{i}{\hbar} S(p, t_2, t_1)} \\ &\times e^{i\omega_{\mathbf{k}} t_1} d_{j',c}^* \left( p - \frac{e}{c} A(t_1) \right) a_{j'}^{(0)}(t_1), \end{aligned} \quad (38)$$

where we have that the photon of frequency  $\omega_{\mathbf{k}}$  is generated at time  $t_1$ , i.e. when the electron gets excited to the conduction band, while at the recombination time no photons are generated. Thus, this process does not have any semiclassical correspondence, and appears only when introducing the quantum optical nature of the field, similarly to the terms that are neglected in the Jaynes-Cummings model via the Rotating-Wave Approximation [68, 75], and which play an important role in Dynamical Casimir Effect [78] like emissions in Dicke superradiant phase transitions [79]. We interpret them as a consequence of the initial vacuum quantum fluctuations.

In Fig. 3, we show the probabilities associated to each of the processes we have just described. We have considered a ZnO system as solid system, as it was shown that there is a weak dependence of the harmonic emission

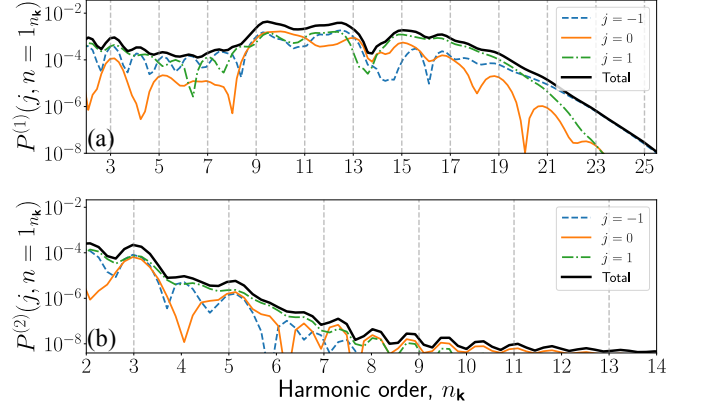


FIG. 3. In (a), we show the (unnormalized) probability of generating an harmonic photon in a process where the photon is generated when the electron recombines to Wannier site  $j$  of the valence band. In (b), we consider the process where the photon is generated when the electron gets excited to the conduction band. We see that in (a) we recover the plateau structure while in (b) the probability decays as the harmonic order of the photon increases. The solid system is ZnO and the laser field has polarization along the  $\Gamma - A$  direction, with 4 cycles of duration, a sinusoidal-squared envelope, central wavelength  $\lambda_L = 3.25 \mu\text{m}$ , and peak intensity  $I_0 = 5 \times 10^{11} \text{ W/cm}^2$ .

with the field's ellipticity, which suggests the influence of delocalized recombination processes [25]. We excite this solid-state system by a laser that has linear polarization along the  $\Gamma - A$  direction, a  $\sin^2$ -shaped envelope, central frequency  $\omega_{\mathbf{k}L} = 0.014 \text{ a.u.}$ , field amplitude  $E_0 = 0.00375 \text{ a.u.}$ , and 4 cycles of total duration. Furthermore, we set  $a = 9.83 \text{ a.u.}$ ,  $I_c = 0.02175 \text{ a.u.}$ ,  $I_v = -0.00295 \text{ a.u.}$  and  $\mathcal{E}_g = 0.1213 \text{ a.u.}$ , and computed all the integrals numerically as explained in Appendix C. Moreover, we have considered that, before getting excited to the conduction band, the electron can travel to fifteen Wannier sites ( $j' \in [-7, 7]$ ), an amount which provides a good convergence for our results. As we can see in Fig. 3 (a), the event described by Eq. (37) provides harmonic photons with almost equal probability until a cutoff frequency located around the 16th harmonic, where the probability starts to decay. This contrasts with what we find in Fig. 3 (b) for the process described by Eq. (38), which leads to similar values of the probability as those shown in Fig. 3 (a) for low harmonics, while for harmonics larger than the 5th the probability decays and does not show a plateau. We also note that, in both cases, there is not a clear even-odd harmonic symmetry, and recombination in the different Wannier sites we considered provide a similar contribution to the final probability of the corresponding process to happen.

The primary conclusion from Fig. 3 is that that the main responsible of the plateau structure in HHG in solids is the mechanism described by  $\mathcal{P}^{(1)}(j, 1_{\mathbf{k}}, t)$ . When combined with the other process as in Eq. (36), we get Fig. 4 (a) which agrees with the harmonic spectrum (see

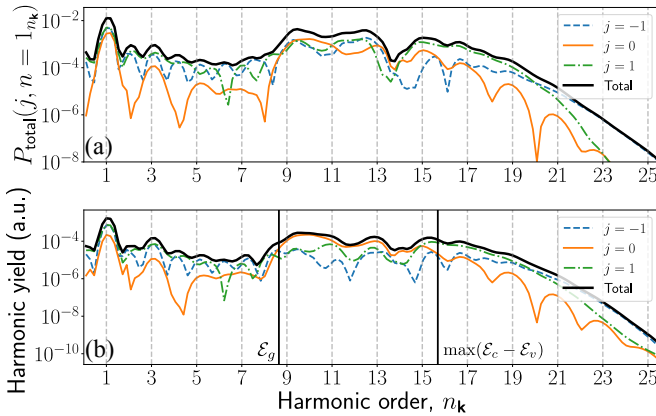


FIG. 4. In (a), we show the (unnormalized) total probability of generating an harmonic photon according to Eq. (36). In (b), we show the semiclassical harmonic spectrum computed as shown in Appendix C. We note that, in (a), the peak at the first corresponds with the probability of generating and a photon of frequency  $\omega_{\mathbf{k}_L}$  by one of the processes presented in Eqs. (37) and (38). The solid system is ZnO and the laser field has polarization along the  $\Gamma - A$  direction, with 4 cycles of duration, a sinusoidal-squared envelope, central wavelength  $\lambda_L = 3.25 \mu\text{m}$ , and peak intensity  $I_0 = 5 \times 10^{11} \text{ W/cm}^2$ .

Appendix C) obtained from the semiclassical picture, and which we show in Fig. 4 (b). Both figures share some features such as the harmonic plateau present from the band gap energy  $\mathcal{E}_g$  (located right before the 9th harmonic) until the maximum energy difference between the bands (located around the 16th harmonic), the stronger peaks for the lowest harmonics, and a no clear identification of an even-odd harmonic symmetry, similarly to what is shown in Ref. [27] for the same solid and laser parameters. However, there are some differences between these two figures, which are mainly due to the different contributions we obtain when the electron recombines in different Wannier sites. In particular, we observe that the structure of the plateau spectrum in Fig. 4 (a) is dominated by recombination effects at site  $j = 0$ , while in Fig. 4 (b) the effect of the different sites provide important contributions as well in the plateau region. These differences lead to a slightly different structure of the plateau, although after the cutoff at  $n_{\mathbf{k}} > \max(\mathcal{E}_c - \mathcal{E}_g)$ , recombination at sites  $j \neq 0$  are dominant in both cases. Finally, the different contributions obtained for recombination sites  $j = 1$  and  $j = -1$  might be due to CEP effects. We expect that, for longer laser pulses, these two contributions to be comparable.

Finally, we remark that in Fig. 4 (a), the peak shown at  $n_{\mathbf{k}} = 1$  comes from evaluating Eqs. (37) and (38) setting  $\omega_{\mathbf{k}} = \omega_{\mathbf{k}_L}$ . Thus, it does not represent the probability of having a single photon in the fundamental mode, but the probability of having a recombination event in which a photon of frequency  $\omega_{\mathbf{k}_L}$  is generated. In order to obtain the probability of having a single photon in the fundamental mode, one has to take into account other events as shown in Appendix D, but we present it this way as it

is particularly useful for the numerical evaluation of the expressions presented in the next section.

### C. Conditioning to HHG

In current experimental implementations, the generation of non-classical states from HHG processes relies on an heralding scheme where a correlation measurement between the harmonics and part of the fundamental mode is carried out [58, 61, 62, 65]. From a mathematical perspective, we look at those events in which at least one harmonic mode is generated, but taking into account the correlations that are established with the fundamental mode. Mathematically speaking, we consider the projective operation [61]

$$\hat{P}_{\text{HHG}} = \mathbb{1} - |\alpha\rangle\langle\alpha| \bigotimes_{\mathbf{k} \in \text{HH}} |\mathbf{0}_{\mathbf{k}}\rangle\langle\mathbf{0}_{\mathbf{k}}|, \quad (39)$$

which we refer to as *conditioning to HHG*. Applying this operation onto Eq. (34), results in

$$\begin{aligned} |\Psi_{\text{cond}}(t)\rangle &= \hat{P}_{\text{HHG}} |\Psi(t)\rangle \\ &\approx |\Psi_{\text{HHG}}(t)\rangle \\ &\quad - \langle \alpha, \{0\}_{\mathbf{k} \in \text{HH}} | \Psi_{\text{HHG}}(t) \rangle |\alpha, \{0\}_{\mathbf{k} \in \text{HH}}\rangle, \end{aligned} \quad (40)$$

which we proceed to characterize in the following subsections under different scenarios.

#### 1. Measuring the XUV modes

In Refs. [58, 65], particular attention was paid to the state of the fundamental after HHG processes in gases. In particular, the presence of non-classical states of light, i.e., with negativities in their Wigner function representation, was reported. For that reason, we consider here the same scenario, but using a solid target as a HHG generating medium instead of an atomic system.

First of all, since from the experimental point of view, and to our knowledge, is not possible to distinguish the Wannier site in which the electron has ended up in, we trace out in Eq. (40) the electronic degrees of freedom. However, for the field modes one can select a range of harmonics to measure by introducing a suitable filter, as done in Refs. [58, 65]. We impose this requirement in our equations by projecting those modes which we do not measure by the vacuum state, such that after tracing out all the harmonic modes that are indeed measured, we get

$$\tilde{\rho}(t) = \text{tr}_{\text{elec}, \mathbf{k} \neq \mathbf{k}_L} \left( \langle \{0\}_{\mathbf{k} \notin \text{filter}} | \rho_{\text{cond}}(t) | \{0\}_{\mathbf{k} \notin \text{filter}} \rangle \right), \quad (41)$$

where we have denoted  $\rho_{\text{cond}}(t) = |\Psi_{\text{cond}}(t)\rangle\langle\Psi_{\text{cond}}(t)|$ , and where the set  $\{\mathbf{k} : \mathbf{k} \notin \text{filter}\}$  represents all those field modes that are eliminated, for instance, by a suitable optical filter. By implementing these operations (see

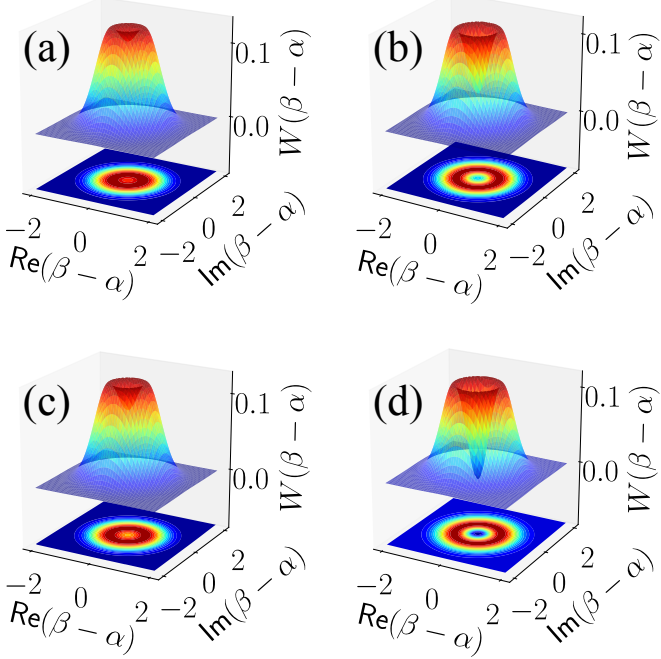


FIG. 5. Wigner functions for conditioning over different harmonic ranges, i.e., those frequencies that are not eliminated by the filter. In (a) we considered the range  $n_{\mathbf{k}} \in [9, 15]$ , in (b) the range  $n_{\mathbf{k}} \in [11, 15]$ , in (c) the range  $n_{\mathbf{k}} \in [9, 13]$  and in (d)  $n_{\mathbf{k}} \in [11, 13]$ . We observe that, the lower the range is, the deeper is the central minimum of the Wigner function.

Appendix E for a step-by-step derivation), we end up with the following state for the fundamental mode

$$\begin{aligned} \tilde{\rho}(t) = & \left( \sum_j P_{\text{total}}(j, 1_{\mathbf{k}_L}, t) \right) D(\alpha) |1_L\rangle\langle 1_L| D^\dagger(\alpha) \\ & + \left( \sum_{j, \mathbf{k} \neq \mathbf{k}_L} P_{\text{total}}(j, 1_{\mathbf{k}}, t) \right) |\alpha\rangle\langle\alpha|, \end{aligned} \quad (42)$$

where  $P_{\text{total}}(j, 1_{\mathbf{k}}, t) = |\sum_{i=1,2} \mathcal{P}^{(i)}(j, 1_{\mathbf{k}}, t)|^2$ . The state we get after these operations is expressed as a maximally mixed state given as the combination between a displaced single-photon state and a coherent state. Following Ref. [80], the Wigner function of this state can be written as

$$\begin{aligned} W(\beta) &= \frac{2}{\pi} \text{tr}(D(\beta)\Pi D(\beta)\tilde{\rho}(t)) \\ &= \frac{2}{\pi} \left[ \left( \sum_j P_{\text{total}}(j, 1_{\mathbf{k}_L}, t) \right) (4|\beta|^2 - 1) \right. \\ &\quad \left. + \sum_{j, \mathbf{k} \neq \mathbf{k}_L} P_{\text{total}}(j, 1_{\mathbf{k}}, t) \right] e^{-2|\beta|^2}. \end{aligned} \quad (43)$$

In Fig. 5, we show the Wigner function presented in Eq. (43) for different harmonic conditionings. More specifically, in Fig. 5 (a) we consider that the measured harmonics, i.e. those ones that are not eliminated by the filter, belong to the range  $n_{\mathbf{k}} \in [9, 15]$ ; in

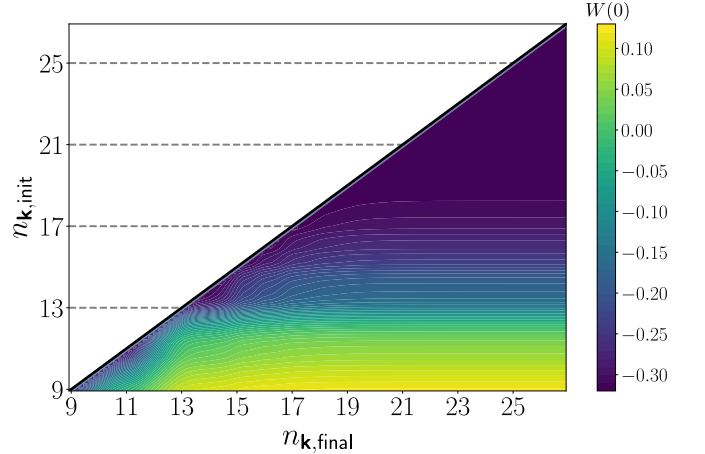


FIG. 6. Central value of the Wigner distribution as a function of the harmonic range  $[n_{\mathbf{k},\text{init}}, n_{\mathbf{k},\text{final}}]$ .

Fig. 5 (b), we use the range  $n_{\mathbf{k}} \in [11, 15]$ ; in Fig. 5 (c), the range  $n_{\mathbf{k}} \in [9, 13]$ ; and finally in Fig. 5 (d), the range  $n_{\mathbf{k}} \in [11, 13]$ . We observe that, the larger the range, the more contribution comes from the coherent state part of Eq. (42). For the longest harmonic ranges, see for example Figs. 5 (a) and (c), the obtained Wigner function has a Gaussian shape with a small minimum at the center, which becomes deeper as the harmonic range decreases, i.e., when the contribution to the displaced single photon state in Eq. (42) becomes more important. Finally, for small ranges as that of Fig. 5 (d), one can potentially find negative regions in the final Wigner function, witnessing the presence of non-classical states of light.

In the figure we have just discussed about, we also observe that similar sizes for the harmonic range lead to slightly different Wigner distributions. For instance, although in Figs. 5 (b) and (d) we have conditioned over the same number of harmonic modes, the obtained minima in the former is deeper than in the latter. This is a consequence of how the probability contributions add up for each harmonic range. Related to the previous ranges, in Fig. 4 (a) we observe that in the range  $n_{\mathbf{k}} \in [9, 13]$  the probability of having a photon in one of the harmonic modes remains constant, while in the range  $n_{\mathbf{k}} \in [11, 15]$  there is minimum around the 14th harmonic mode. Thus, by choosing properly the harmonic range, one could control the purity of the obtained state. In Fig. 6, we show how the central value of the Wigner distribution, i.e.  $W(\beta - \alpha = 0)$ , behaves as a function of the harmonic range that is used for the conditioning. In particular, we have considered a range of harmonic modes  $n_{\mathbf{k}} \in [n_{\mathbf{k},\text{init}}, n_{\mathbf{k},\text{final}}]$ , and changed both limiting values of the range. In general, we observe that the bigger the range, the more positive the central part of the Wigner function is. We also observe that, when keeping  $n_{\mathbf{k},\text{init}}$  constant, the central value of the Wigner function converges to some value when increasing  $n_{\mathbf{k},\text{final}}$ , which depends on the specific initial harmonic that is considered.

These are consequences of the fact that the probability of having a photon in an harmonic mode beyond the cutoff dramatically decreases, as shown in Fig. 4 (a). Therefore, when the size of the considered range is small enough and located at the right hand side part of the cutoff frequency, most of the contribution in Eq. (42) comes from a displaced Fock state and, therefore, the value of Wigner function at the center is negative.

## 2. Measuring the fundamental mode

In a similar basis to what was presented in Refs. [61, 64], one could experimentally condition on the state of the fundamental instead of the XUV modes, such that non-classical states of light could be potentially obtained in the latter. Based on this, we project the fundamental mode onto  $|\alpha\rangle$  so that Eq. (40) reads

$$\begin{aligned} |\Psi_{\text{cond}}^{(\text{XUV})}\rangle &= \langle\alpha|\Psi_{\text{cond}(t)}\rangle \\ &= \sum_{j,\mathbf{k}} \mathcal{P}_{\text{total}}(j, 1_{\mathbf{k}}, t) |1_{\mathbf{k}}\rangle |\{0\}_{\mathbf{k}' \neq \mathbf{k}}\rangle |w_{v,j}\rangle, \end{aligned} \quad (44)$$

where  $\mathcal{P}_{\text{total}}(j, 1_{\mathbf{k}}, t) = \sum_{i=1,2} \mathcal{P}^{(i)}(j, 1_{\mathbf{k}}, t)$ . This state, presents correlations between the electronic and the different quantum optical components, which could potentially lead to the generation of an *hybrid* entangled state [81] between the electronic and quantum optical degrees of freedom, but also to an entangled state between the different field modes.

We first start by studying the light-matter entanglement present in Eq. (44). Since at this point we are dealing with a pure state, we can use as entanglement measure the entropy of entanglement defined as [82, 83]

$$S(\rho) := -\text{tr}(\rho \log(\rho)), \quad (45)$$

where  $\rho$  is the reduced density matrix of the system. For simplicity, in order to perform the numerical computations we restrict the total number of sites where the electron can end up to three, i.e. we work with the set of Wannier states  $\{|w_{v,-1}\rangle, |w_{v,0}\rangle, |w_{v,1}\rangle\}$ , such that the reduced density matrix with respect to the XUV modes has size  $3 \times 3$  (see Appendix F 1 for more details).

In Fig. 7, we present the obtained results in form of a surface plot in (a), and a contour plot in (b). Here, we study the amount of entanglement as a function of the frequency range  $O = [\omega_{\mathbf{k},\text{init}}, \omega_{\mathbf{k},\text{final}}]$  that is measured, i.e., those modes that are not eliminated by the filter. Thus, the state whose entanglement we characterize is given by  $|\tilde{\Psi}_{\text{cond}}^{(\text{XUV})}\rangle = \langle\{0\}_{\mathbf{k} \notin O}|\Psi_{\text{cond}}^{(\text{XUV})}\rangle$ . We see that, for all cases, we get  $S(\rho) \neq 0$  which implies that the state presented in Eq. (44) shows non-classical correlations between the electronic and quantum optical degrees of freedom. In particular, we see that  $S(\rho)$  reaches its maximum value the larger the range  $O$  is. This is a consequence of the fact that each of the recombining sites  $j$  contribute differently to the harmonic emission

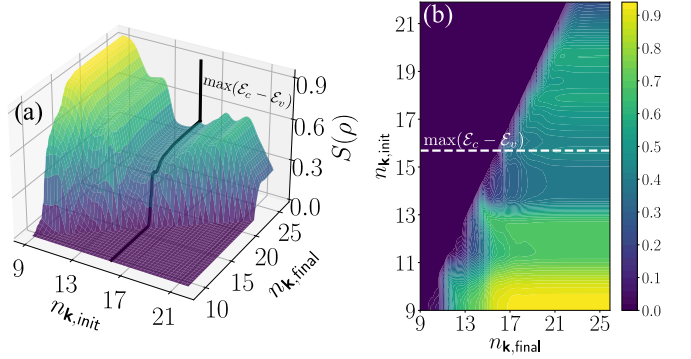


FIG. 7. Entropy of entanglement between the electronic degrees of freedom and a given frequency range  $O = [\omega_{\mathbf{k},\text{init}}, \omega_{\mathbf{k},\text{final}}]$  containing those modes that are not eliminated by a filter. Here, we define  $n_{\mathbf{k},\text{init}} = \omega_{\mathbf{k},\text{init}}/\omega_{\mathbf{k}_L}$  and  $n_{\mathbf{k},\text{final}} = \omega_{\mathbf{k},\text{final}}/\omega_{\mathbf{k}_L}$ . In (a) we show a surface plot of  $S(\rho)$  while in (b) we show a contour plot of the same quantity. The black solid curve in (a) and the dashed white curve in (b) show the location of the maximum energy difference between the conduction and valence band. For  $n_{\mathbf{k},\text{init}} > n_{\mathbf{k},\text{final}}$  we have that  $S(\rho)$  is not defined, and for numerical reasons we have set the values in these regime to zero.

for the different frequencies that we can get after HHG. Mathematically speaking, an increase in the harmonic range makes the quantum optical component associated to each  $|w_{v,j}\rangle$  more different, to the extent that their overlap becomes very small. On the other hand, we observe that the greatest value of  $S(\rho)$  is obtained when  $\omega_{\mathbf{k},\text{init}}/\omega_{\mathbf{k}_L} = n_{\mathbf{k},\text{init}} = 9$ , and decreases until it reaches the maximum value of the energy difference between the conduction and valence band (represented by the black curve in Fig. 7 (a) and with the dashed white line in Fig. 7 (b)). Afterwards, it experiences a small enhancement until  $n_{\mathbf{k},\text{init}} \approx 21$ , after which it starts to decrease again. We note that, in this regime, we are far within the cutoff region of the spectrum, where we observe in Fig. 4 (a) that most of the contribution to the state comes from site  $j = -1$ , leading to a very close to separable state and, therefore, to a decreasing value of  $S(\rho)$ .

Let us consider now the case where the electronic degrees of freedom are disregarded. We first note that, if we consider the case where the electron is found in a given Wannier site  $|w_{v,j}\rangle$ , the corresponding projective operation leaves Eq. (44) in a pure state where an harmonic excitation is delocalized in one of the possible modes, that is

$$\begin{aligned} |\Psi_{\text{cond},j}^{(\text{XUV})}\rangle &= \langle w_{v,j}|\Psi_{\text{cond}}^{(\text{XUV})}\rangle \\ &= \sum_{\mathbf{k}} \mathcal{P}_{\text{total}}(j, 1_{\mathbf{k}}, t) |1_{\mathbf{k}}\rangle |\{0\}_{\mathbf{k}' \neq \mathbf{k}}\rangle. \end{aligned} \quad (46)$$

Note that the obtained states after the projective operation bears some similarity with the so-called *generalized*

$W$  states [84], which are defined as

$$|W_M\rangle = \frac{1}{\sqrt{M}} \sum_n |1_n\rangle |\{0\}_{n' \neq n}\rangle, \quad (47)$$

where the excitation can be found with equal probability in each of the possible modes  $n$ . Hereupon, we will refer to the state in Eq. (47) as a  $W$  state of length  $M$ . These class of  $W$  states are in general multipartite entangled [85, 86] and, furthermore, present strong nonlocal features [87, 88]. This makes them a perfect candidate for different applications of quantum information science such as teleportation protocols [89–91], as well as superdense coding [92], and quantum communication [93–95]. Thus, their widespread use motivates the performance of a comparison about how close the states in Eq. (46) are from the one presented in Eq. (47). However, and to our knowledge, from an experimental point of view it is not possible to know in which Wannier site the electron has ended up in. Thus, we also consider the case where the electronic degrees of freedom are traced out, such that we are left with the following mixed state

$$\rho^{(\text{XUV})} = \sum_{j,\mathbf{k},\tilde{\mathbf{k}}} \mathcal{P}_{\text{total}}(j, 1_{\mathbf{k}}, t) \mathcal{P}_{\text{total}}^*(j, 1_{\tilde{\mathbf{k}}}, t) \\ \times |1_{\mathbf{k}}\rangle\langle 1_{\tilde{\mathbf{k}}}| \otimes |\{0\}_{\mathbf{k}' \neq \mathbf{k}}\rangle\langle \{0\}_{\tilde{\mathbf{k}}' \neq \tilde{\mathbf{k}}}|. \quad (48)$$

In order to determine how close the states in Eqs. (46) and (48) are from a  $W$  state of length  $M$ , we use the fidelity as a measure of *closeness* between two quantum states, which is defined as [83]

$$F(\sigma, \rho) := \left[ \text{tr} \left( \sqrt{\sqrt{\sigma} \rho \sqrt{\sigma}} \right) \right]^2, \quad (49)$$

and given by (see Appendix F 2 for details)

$$F(|W_M\rangle, |\Psi_{\text{cond},j}^{(\text{XUV})}\rangle) = \frac{1}{M} \left| \sum_{\mathbf{k}} \mathcal{P}_{\text{total}}(j, 1_{\mathbf{k}}, t) \right|^2 \quad (50)$$

for the pure state in Eq. (46), while for the mixed state in Eq. (48) as

$$F(|W_M\rangle, \rho^{(\text{XUV})}) = \frac{1}{M} \sum_{j,\mathbf{k},\tilde{\mathbf{k}}} \mathcal{P}_{\text{total}}(j, 1_{\mathbf{k}}, t) \mathcal{P}_{\text{total}}^*(j, 1_{\tilde{\mathbf{k}}}, t). \quad (51)$$

Note that, in order to perform a comparison with a generalized  $W$  state of length  $M$ , we first need to bound the number of modes in the quantum optical states presented in Eqs. (46) and (48). We consider here two approaches. The first one consists on defining a range of harmonic modes  $O_n = [n_{\mathbf{k},\text{init}}, n_{\mathbf{k},\text{final}}]$ , such that  $M$  is given by the length of the interval, that is,  $M = \|O_n\|$ . All the other modes that are not included in the considered interval are projected onto a vacuum state, as if they were eliminated by means of a filter. Thus, by changing

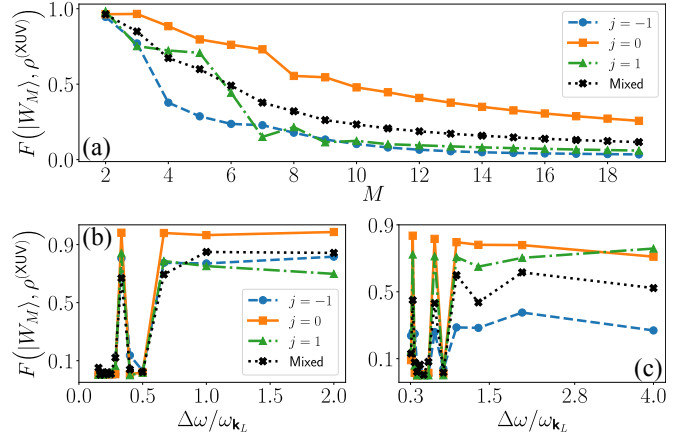


FIG. 8. Fidelity of the pure state in Eq. (46) and of the mixed state in Eq. (48) with respect to a  $W$  state of length  $M$ . We consider two approaches for defining the length  $M$  of the state. In (a), we define a range of harmonic modes  $O_n = [n_{\mathbf{k},\text{init}}, n_{\mathbf{k},\text{final}}]$ , where  $n_{\mathbf{k},\text{init}} = 9$  and  $n_{\mathbf{k},\text{final}}$  has been changed from the 10th to the 27th harmonic, such that  $M = \|O_n\|$ . On the other hand, in (b) and (c) we define a range of frequencies  $O_{\omega} = \{\omega_{\mathbf{k}_1}, \dots, \omega_{\mathbf{k}_M}\}$ , where we have set  $\omega_{\mathbf{k}_1}/\omega_{\mathbf{k}_L} = 9$  while  $\omega_{\mathbf{k}_M}/\omega_{\mathbf{k}_L} = 11$  in (b) and  $\omega_{\mathbf{k}_M}/\omega_{\mathbf{k}_L} = 13$  in (c). The difference between two consecutive frequencies in the set is then given by  $\Delta\omega = (\omega_{\mathbf{k},M} - \omega_{\mathbf{k},1})/(M - 1)$ .

the values  $n_{\mathbf{k},\text{init}}$  and  $n_{\mathbf{k},\text{final}}$ , we can control  $M$ . The second choice is to consider a set of frequencies  $O_{\omega} = \{\omega_{\mathbf{k}_1}, \dots, \omega_{\mathbf{k}_M}\}$ , where  $\omega_{\mathbf{k}_{i+1}} = \omega_{\mathbf{k}_i} + \Delta\omega$ . In this case, we fix the values of  $\omega_{\mathbf{k}_1}$  and  $\omega_{\mathbf{k}_M}$ , and vary the value of  $\Delta\omega$  by changing  $M$ , such that the relation between these two quantities is given by  $\Delta\omega = (\omega_{\mathbf{k},M} - \omega_{\mathbf{k},1})/(M - 1)$ . Similarly to the previous case, all the modes that are not included in the set  $O_{\omega}$  are projected onto a vacuum state. Note that, although similar, the two approaches we consider here are different in the sense that in the first one an increase in  $M$  implies an increase in the difference between the initial and final frequencies of the interval, while in the second it implies the introduction of more frequencies within a fixed interval. Thus, the implementation of the second one would require photodetectors able to distinguish between two frequencies that differ in  $\Delta\omega$ , where an increase in  $M$  implies a reduction on this frequency difference.

In Fig. 8, we show how the fidelity behaves for each of the cases presented before. The first scenario considered, where the range  $O_n$  is defined, is shown in Fig. 8 (a). Here, we have set  $n_{\mathbf{k},\text{init}} = 9$  and varied  $n_{\mathbf{k},\text{final}}$  from the 10th to the 27th harmonic mode. We observe that, the lower  $M$  is, the closer the obtained state is to a  $|W_M\rangle$  state. As more harmonic modes are considered, the fidelity decreases as well since the probability amplitudes in the final superposition are less homogeneous. In particular, we observe that for very large values of  $M$ , the fidelity tends to zero as we are introducing frequencies that are beyond the cutoff, and for which the probability of finding a photon in this frequency regime tends to

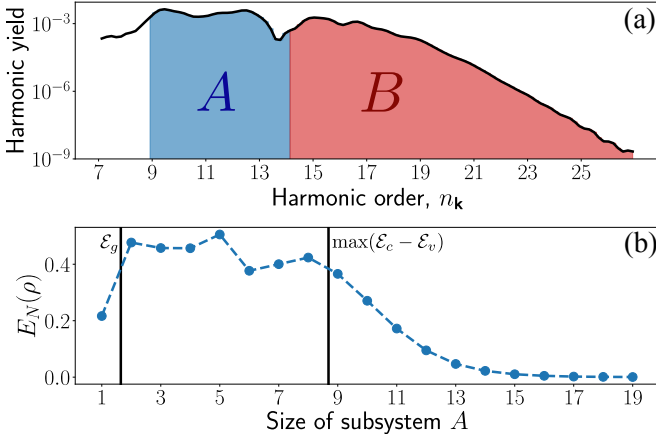


FIG. 9. In order to study the entanglement between the XUV modes, we consider a bipartition of the harmonic spectrum in two subsystems,  $A$  and  $B$ , as shown in (a). This allows us to characterize the entanglement between the subsystems by means of the logarithmic negativity as a function of the size of subsystem  $A$  (or equivalently subsystem  $B$ ), which is defined as the number of harmonics it contains. Here, the first harmonic we consider is the 8th, and the last one is the 27th. The horizontal black lines denote the energy bandgap and the maximum energy between the conduction and valence band, from left to right respectively.

zero. As expected, we also observe that the fidelity of the mixed state is always below the maximum fidelity obtained by one of the three pure states we consider.

On the other hand, in Figs. 8 (b) and (c), we consider the case where the range  $O_\omega$  is defined. In both cases, we have set  $\omega_{\mathbf{k},1}/\omega_{\mathbf{k}_L} = 9$ , while the final value is different for each of the plots, concretely  $\omega_{\mathbf{k},1}/\omega_{\mathbf{k}_L} = 11$  and  $\omega_{\mathbf{k},1}/\omega_{\mathbf{k}_L} = 13$ , respectively for (b) and (c). We observe in both cases that the fidelity remains close to one for decreasing values of  $\Delta\omega$ , i.e., increasing values of  $M$ . This contrasts with what is observed in Fig. 8 (a), and is a consequence of the frequency regime that is being considered. Looking at Fig. 4 (a), in these two cases we are restricting ourselves to regimes of frequencies where the probability of finding a photon in the harmonic modes is more homogeneous and, hence, leads to higher values of the fidelity. We also observe in both cases huge jumps in the fidelity for small values of  $\Delta\omega$ , which are due to the highly oscillating nature of the corresponding probability amplitudes.

Finally, to conclude with this section, we study the entanglement structure of the state presented in Eq. (48). In particular, the considered state presents a multipartite entanglement structure, where all the field modes are correlated. However, the entanglement characterization of these states is still an open problem, and has been studied in specific scenarios (see for instance Ref. [82] and references therein). Here, with the aim of quantifying the entanglement between the XUV modes, we are going to consider the well-known bipartite scenario, such that we split the harmonic spectrum in two parts

$A$  and  $B$ , as shown in Fig. 9 (a). Thus, subsystem  $A$  contains all the harmonic modes within the interval  $O_A = [n_{\mathbf{k},\text{init}}^{(A)}, n_{\mathbf{k},\text{final}}^{(A)}]$ , while subsystem  $B$  contains all the modes within the interval  $O_B = [n_{\mathbf{k},\text{init}}^{(B)}, n_{\mathbf{k},\text{final}}^{(B)}]$ . Hence, under this framework, the logarithmic negativity [82] allows us to study the entanglement between a bipartite system that is in a mixed state. This entanglement measure is defined as

$$E_N(\rho_{AB}) := \log_2(2N(\rho_{AB}) + 1), \quad (52)$$

where  $N(\rho)$  is the *negativity* of  $\rho$ , i.e., the absolute value of the sum of all negative eigenvalues of the partial transpose of  $\rho$  with respect to one of the subsystems [96]. In Fig. 9 (b), we show how the logarithmic negativity behaves as a function of the size of subsystem  $A$ . We observe that this entanglement measure remains almost constant when we consider frequencies that are within the energy bandgap  $E_g$  and the maximum energy difference between the conduction and valence band. In this case, the relative probability of finding an excitation at either subsystem  $A$  or subsystem  $B$  is similar, and therefore the logarithmic negativity remains constant. As the size of subsystem  $A$  comprises the whole harmonic plateau and beyond, the amount of entanglement in the state decreases as the contribution from subsystem  $B$  becomes negligible. Thus, in this case the state is very well approximated by the state of subsystem  $A$ , and the logarithmic negativity vanishes.

Therefore, we observe that opposite restrictions on the harmonic modes leads to two non-exclusive indications of non-classical behaviors, namely the presence of Wigner function negativities and entanglement features.

#### IV. CONCLUSIONS

In this work, we have presented a quantum optical analysis of high-harmonic generation using a Wannier-Bloch description to model the electronic degrees of freedom. This approach has allowed us to further study the process of high-order harmonic generation in solid-state systems under a different perspective, compared to previous semiclassical studies. Firstly, we focused on the HHG process itself. Within this framework, we found that intraband and interband electronic transitions affect differently the quantum optical state of the system. Moreover, we observed that intraband transitions within the conduction and valence band lead to different displacements on the quantum optical state of the field, although comparable in the order of magnitude. We also found that the contribution to the harmonic photons due to interband transitions has two possible sources. One of them is related to the recombination process itself while the other is due to the quantum fluctuations in the initial vacuum state of the XUV modes. Nevertheless, and as expected, the former are more dominant over the latter specially for the high-order harmonics.

Secondly, we studied how the conditioning operations implemented experimentally in Refs. [58, 65] affect the quantum optical state of the system. When the harmonics are measured, we found that the quantum optical state of the fundamental lies in a mixed state between a displaced Fock state and a coherent state. The non-classical features of this state depend on how the conditioning over the XUV modes is performed. On the other hand, when the fundamental modes are measured instead, we find a hybrid entangled state between the electronic degrees of freedom and the XUV modes. If the former are traced out, we are left with an entangled mixed state which bears some analogy to  $W$ -class states, and whose entanglement we studied in a bipartite scenario.

A natural extension of the present work would involve the introduction of decoherence affects within the solid. This would affect not only the harmonic emission, as shown in Refs. [97] and in Appendix G, but also the purity of the final state after the conditioning, which would require different entanglement measures to the ones presented here, in particular for studying the entanglement between the electronic and quantum optical degrees of freedom. However, we expect the observables that involve only the quantum optical state of the light, where the electronic degrees of freedom have been traced out, to get modified only to the extent of how the harmonic emission differs in each of the cases. This would imply that, in our case, we would obtain Wigner negativities for a different range of harmonic conditionings.

In conclusion, this study further extends, at the theoretical level, the applicability of the techniques that have been developed so far for the generation of non-classical states of light in gaseous HHG processes, to solid-state systems. Although our study is based on the dynamics found by solving the Schrödinger equation at the single-electron level, we expect the features we have observed to be present in a multielectron scenario, similarly to what happens with atomic ensembles. Thus, this work sets a basis on how intriguing the quantum optical features arising from strong laser-matter interactions in solids, together with the corresponding conditioning operations, could potentially be.

## ACKNOWLEDGEMENTS

We acknowledge Enky Oudot for enlightening discussions and Themistoklis Mavrogordatos for valuable comments on the manuscript.

ICFO group acknowledges support from: ERC AdG NOQIA; Agencia Estatal de Investigación (R&D project CEX2019-000910-S, funded by MCIN/AEI/10.13039/501100011033, Plan National FIDEUA PID2019-106901GB-I00, FPI, QUANTERA MAQS PCI2019-111828-2, QUANTERA DYNAMITE PCI2022-132919, Proyectos de I+D+I “Retos Colaboración” QUSPIN RTC2019-007196-7); Fundació Cellex; Fun-

dació Mir-Puig; Generalitat de Catalunya through the European Social Fund FEDER and CERCA program (AGAUR Grant No. 2017 SGR 134, QuantumCAT U16-011424, co-funded by ERDF Operational Program of Catalonia 2014-2020); the computer resources and technical support at Barcelona Supercomputing Center MareNostrum (FI-2022-1-0042); EU Horizon 2020 FET-OPEN OPTOlogic (Grant No 899794); National Science Centre, Poland (Symfonia Grant No. 2016/20/W/ST4/00314); European Union’s Horizon 2020 research and innovation programme under the Marie-Skłodowska-Curie grant agreement No 101029393 (STREDCH) and No 847648 (“La Caixa” Junior Leaders fellowships ID100010434: LCF/BQ/PI19/11690013, LCF/BQ/PI20/11760031, LCF/BQ/PR20/11770012, LCF/BQ/PR21/11840013); the Government of Spain (FIS2020-TRANQI and Severo Ochoa CEX2019-000910-S).

P. Tzallas group at FORTH acknowledges LASER-LABEUROPE V (H2020-EU.1.4.1.2 grant no.871124), FORTH Synergy Grant AgiIDA (grand no. 00133), the H2020 framework program for research and innovation under the NEP-Europe-Pilot project (no. 101007417). ELI-ALPS is supported by the European Union and co-financed by the European Regional Development Fund (GINOP Grant No. 2.3.6-15-2015-00001).

J.R-D. acknowledges support from the Secretaria d’Universitats i Recerca del Departament d’Empresa i Coneixement de la Generalitat de Catalunya, as well as the European Social Fund (L’FSE inverteix en el teu futur)-FEDER. P.S. acknowledges funding from the European Union’s Horizon 2020 research and innovation programme under the Marie Skłodowska-Curie grant agreement No 847517. A.S.M. acknowledges funding support from the European Union’s Horizon 2020 research and innovation programme under the Marie Skłodowska-Curie grant agreement, SSFI No. 887153. E.P. acknowledges the Royal Society for University Research Fellowship funding under URF\R1\211390. M.F.C. acknowledges financial support from the Guangdong Province Science and Technology Major Project (Future functional materials under extreme conditions - 2021B0301030005).

## References

- [1] D. M. Villeneuve, Attosecond science, *Contemporary Physics* **59**, 47 (2018).
- [2] M. F. Ciappina, J. A. Pérez-Hernández, A. S. Landsman, W. A. Okell, S. Zherebtsov, B. Först, J. Schötz, L. Seiffert, T. Fennel, T. Shaaran, T. Zimmermann, A. Chacón, R. Guichard, A. Zaïr, J. W. G. Tisch, J. P. Marangos, T. Witting, A. Braun, S. A. Maier, L. Roso, M. Krüger, P. Hommelhoff, M. F. Kling, F. Krausz, and M. Lewenstein, Attosecond physics at the nanoscale, *Reports on Progress in Physics* **80**, 054401 (2017).
- [3] K. Amini, J. Biegert, F. Calegari, A. Chacón, M. F. Ciappina, A. Dauphin, D. K. Efimov, C. F. d. M. Faria, K. Giergiel, P. Gniewek, A. S. Landsman, M. Lesiuk,

- M. Mandrysz, A. S. Maxwell, R. Moszyński, L. Ortmann, J. A. Pérez-Hernández, A. Picón, E. Pisanty, J. Prauzner-Bechcicki, K. Sacha, N. Suárez, A. Zaïr, J. Zakrzewski, and M. Lewenstein, Symphony on strong field approximation, *Reports on Progress in Physics* **82**, 116001 (2019).
- [4] F. Krausz and M. Ivanov, Attosecond physics, *Reviews of Modern Physics* **81**, 163 (2009).
- [5] Y. Kobayashi, T. Sekikawa, Y. Nabekawa, and S. Watanabe, 27-fs extreme ultraviolet pulse generation by high-order harmonics, *Optics Letters* **23**, 64 (1998).
- [6] K. Midorikawa, Y. Nabekawa, and A. Suda, XUV multiphoton processes with intense high-order harmonics, *Progress in Quantum Electronics* **32**, 43 (2008).
- [7] N. Tsatrafyllis, B. Bergues, H. Schröder, L. Veisz, E. Skantzakis, D. Gray, B. Bodi, S. Kuhn, G. D. Tsakiris, D. Charalambidis, and P. Tzallas, The ion microscope as a tool for quantitative measurements in the extreme ultraviolet, *Scientific Reports* **6**, 21556 (2016).
- [8] S. Chatziathanasiou, S. Kahaly, E. Skantzakis, G. Sansone, R. Lopez-Martens, S. Haessler, K. Varju, G. D. Tsakiris, D. Charalambidis, and P. Tzallas, Generation of Attosecond Light Pulses from Gas and Solid State Media, *Photonics* **4**, 26 (2017).
- [9] B. Bergues, D. E. Rivas, M. Weidman, A. A. Muschet, W. Helml, A. Guggenmos, V. Pervak, U. Kleineberg, G. Marcus, R. Kienberger, D. Charalambidis, P. Tzallas, H. Schröder, F. Krausz, and L. Veisz, Tabletop nonlinear optics in the 100-eV spectral region, *Optica* **5**, 237 (2018).
- [10] A. Nayak, I. Orfanos, I. Makos, M. Dumergue, S. Kühn, E. Skantzakis, B. Bodi, K. Varju, C. Kalpouzos, H. I. B. Banks, A. Emmanouilidou, D. Charalambidis, and P. Tzallas, Multiple ionization of argon via multi-XUV-photon absorption induced by 20-GW high-order harmonic laser pulses, *Physical Review A* **98**, 023426 (2018).
- [11] B. Senftleben, M. Kretschmar, A. Hoffmann, M. Sauppe, J. Tümmeler, I. Will, T. Nagy, M. J. J. Vrakking, D. Rupp, and B. Schütte, Highly non-linear ionization of atoms induced by intense high-harmonic pulses, *Journal of Physics: Photonics* **2**, 034001 (2020).
- [12] I. Orfanos, I. Makos, I. Lontos, E. Skantzakis, B. Major, A. Nayak, M. Dumergue, S. Kühn, S. Kahaly, K. Varju, G. Sansone, B. Witzel, C. Kalpouzos, L. A. A. Nikolopoulos, P. Tzallas, and D. Charalambidis, Non-linear processes in the extreme ultraviolet, *Journal of Physics: Photonics* **2**, 042003 (2020).
- [13] C. Gohle, T. Udem, M. Herrmann, J. Rauschenberger, R. Holzwarth, H. A. Schuessler, F. Krausz, and T. W. Hänsch, A frequency comb in the extreme ultraviolet, *Nature* **436**, 234 (2005).
- [14] A. Cingöz, D. C. Yost, T. K. Allison, A. Ruehl, M. E. Fermann, I. Hartl, and J. Ye, Direct frequency comb spectroscopy in the extreme ultraviolet, *Nature* **482**, 68 (2012).
- [15] T. Popmintchev, M.-C. Chen, D. Popmintchev, P. Arpin, S. Brown, S. Ališauskas, G. Andriukaitis, T. Balčiunas, O. D. Mücke, A. Pugzlys, A. Baltuška, B. Shim, S. E. Schrauth, A. Gaeta, C. Hernández-García, L. Plaja, A. Becker, A. Jaron-Becker, M. M. Murnane, and H. C. Kapteyn, Bright Coherent Ultra-high Harmonics in the keV X-ray Regime from Mid-Infrared Femtosecond Lasers, *Science* **336**, 1287 (2012).
- [16] J. L. Krause, K. J. Schafer, and K. C. Kulander, High-order harmonic generation from atoms and ions in the high intensity regime, *Physical Review Letters* **68**, 3535 (1992).
- [17] P. B. Corkum, Plasma perspective on strong field multiphoton ionization, *Physical Review Letters* **71**, 1994 (1993).
- [18] K. C. Kulander, K. J. Schafer, and J. L. Krause, Dynamics of short-pulse excitation, ionization and harmonic conversion, in *Super-Intense Laser Atom Physics*, NATO Advanced Studies Institute Series B: Physics, Vol. 316, edited by B. Piraux, A. L'Huillier, and K. Rzążewski (Plenum, New York, 1993) pp. 95–110.
- [19] M. Lewenstein, P. Balcou, M. Y. Ivanov, A. L'Huillier, and P. B. Corkum, Theory of high-harmonic generation by low-frequency laser fields, *Physical Review A* **49**, 2117 (1994).
- [20] S. Y. Kruchinin, F. Krausz, and V. S. Yakovlev, Colloquium: Strong-field phenomena in periodic systems, *Reviews of Modern Physics* **90**, 021002 (2018).
- [21] S. Ghimire and D. A. Reis, High-harmonic generation from solids, *Nature Physics* **15**, 10 (2019).
- [22] J. Park, A. Subramani, S. Kim, and M. F. Ciappina, Recent trends in high-order harmonic generation in solids, *Advances in Physics: X* **7**, 2003244 (2022).
- [23] G. Vampa, C. McDonald, G. Orlando, D. Klug, P. Corkum, and T. Brabec, Theoretical Analysis of High-Harmonic Generation in Solids, *Physical Review Letters* **113**, 073901 (2014).
- [24] G. Vampa, C. R. McDonald, G. Orlando, P. B. Corkum, and T. Brabec, Semiclassical analysis of high harmonic generation in bulk crystals, *Physical Review B* **91**, 064302 (2015).
- [25] S. Ghimire, A. D. DiChiara, E. Sistrunk, P. Agostini, L. F. DiMauro, and D. A. Reis, Observation of high-order harmonic generation in a bulk crystal, *Nature Physics* **7**, 138 (2011).
- [26] G. Ndabashimiye, S. Ghimire, M. Wu, D. A. Browne, K. J. Schafer, M. B. Gaarde, and D. A. Reis, Solid-state harmonics beyond the atomic limit, *Nature* **534**, 520 (2016).
- [27] E. N. Osika, A. Chacón, L. Ortmann, N. Suárez, J. A. Pérez-Hernández, B. Szafran, M. F. Ciappina, F. Sols, A. S. Landsman, and M. Lewenstein, Wannier-Bloch Approach to Localization in High-Harmonics Generation in Solids, *Physical Review X* **7**, 021017 (2017).
- [28] F. H. M. Faisal and J. Z. Kamiński, Floquet-Bloch theory of high-harmonic generation in periodic structures, *Physical Review A* **56**, 748 (1997).
- [29] A. K. Gupta, O. E. Alon, and N. Moiseyev, Generation and control of high-order harmonics by the interaction of an infrared laser with a thin graphite layer, *Physical Review B* **68**, 205101 (2003).
- [30] D. Golde, T. Meier, and S. W. Koch, High harmonics generated in semiconductor nanostructures by the coupled dynamics of optical inter- and intraband excitations, *Physical Review B* **77**, 075330 (2008).
- [31] D. Golde, T. Meier, and S. W. Koch, Microscopic analysis of high-harmonic generation in semiconductor nanostructures, *physica status solidi c* **6**, 420 (2009).
- [32] S. Ghimire, A. D. DiChiara, E. Sistrunk, G. Ndabashimiye, U. B. Szafruga, A. Mohammad, P. Agostini, L. F. DiMauro, and D. A. Reis, Generation and propagation of high-order harmonics in crystals, *Physi-*

- cal Review A **85**, 043836 (2012).
- [33] T. Higuchi, M. I. Stockman, and P. Hommelhoff, Strong-Field Perspective on High-Harmonic Radiation from Bulk Solids, *Physical Review Letters* **113**, 213901 (2014).
- [34] C. R. McDonald, G. Vampa, P. B. Corkum, and T. Brabec, Interband Bloch oscillation mechanism for high-harmonic generation in semiconductor crystals, *Physical Review A* **92**, 033845 (2015).
- [35] M. Wu, S. Ghimire, D. A. Reis, K. J. Schafer, and M. B. Gaarde, High-harmonic generation from Bloch electrons in solids, *Physical Review A* **91**, 043839 (2015).
- [36] G. Vampa, C. McDonald, A. Fraser, and T. Brabec, High-Harmonic Generation in Solids: Bridging the Gap Between Attosecond Science and Condensed Matter Physics, *IEEE Journal of Selected Topics in Quantum Electronics* **21**, 1 (2015).
- [37] T. T. Luu and H. J. Wörner, High-order harmonic generation in solids: A unifying approach, *Physical Review B* **94**, 115164 (2016).
- [38] T. Tamaya, A. Ishikawa, T. Ogawa, and K. Tanaka, Diabatic Mechanisms of Higher-Order Harmonic Generation in Solid-State Materials under High-Intensity Electric Fields, *Physical Review Letters* **116**, 016601 (2016).
- [39] C. Yu, X. Zhang, S. Jiang, X. Cao, G. Yuan, T. Wu, L. Bai, and R. Lu, Dependence of high-order-harmonic generation on dipole moment in SiO<sub>2</sub> crystals, *Physical Review A* **94**, 013846 (2016).
- [40] S. Jiang, H. Wei, J. Chen, C. Yu, R. Lu, and C. D. Lin, Effect of transition dipole phase on high-order-harmonic generation in solid materials, *Physical Review A* **96**, 053850 (2017).
- [41] T.-Y. Du, D. Tang, X.-H. Huang, and X.-B. Bian, Multichannel high-order harmonic generation from solids, *Physical Review A* **97**, 043413 (2018).
- [42] N. Tancogne-Dejean and A. Rubio, Atomic-like high-harmonic generation from two-dimensional materials, *Science Advances* **4**, eaao5207 (2018).
- [43] S. Jiang, J. Chen, H. Wei, C. Yu, R. Lu, and C. Lin, Role of the Transition Dipole Amplitude and Phase on the Generation of Odd and Even High-Order Harmonics in Crystals, *Physical Review Letters* **120**, 253201 (2018).
- [44] S. Jiang, S. Gholam-Mirzaei, E. Crites, J. E. Beetar, M. Singh, R. Lu, M. Chini, and C. D. Lin, Crystal symmetry and polarization of high-order harmonics in ZnO, *Journal of Physics B: Atomic, Molecular and Optical Physics* **52**, 225601 (2019).
- [45] R. E. F. Silva, A. Jiménez-Galán, B. Amorim, O. Smirnova, and M. Ivanov, Topological strong-field physics on sub-laser-cycle timescale, *Nature Photonics* **13**, 849 (2019).
- [46] L. Yue and M. B. Gaarde, Imperfect Recollisions in High-Harmonic Generation in Solids, *Physical Review Letters* **124**, 153204 (2020).
- [47] C. Yu, S. Jiang, T. Wu, G. Yuan, Y. Peng, C. Jin, and R. Lu, Higher harmonic generation from bilayer nanostructures assisted by electron backscattering, *Physical Review B* **102**, 241407 (2020).
- [48] S. Jiang, C. Yu, J. Chen, Y. Huang, R. Lu, and C. D. Lin, Smooth periodic gauge satisfying crystal symmetry and periodicity to study high-harmonic generation in solids, *Physical Review B* **102**, 155201 (2020).
- [49] P. Jürgens, B. Liewehr, B. Kruse, C. Peltz, D. Engel, A. Husakou, T. Witting, M. Ivanov, M. J. J. Vrakking, T. Fennel, and A. Mermilliod-Blondin, Origin of strong-field-induced low-order harmonic generation in amorphous quartz, *Nature Physics* **16**, 1035 (2020).
- [50] S. Imai, A. Ono, and S. Ishihara, High Harmonic Generation in a Correlated Electron System, *Physical Review Letters* **124**, 157404 (2020).
- [51] N. Marzari, A. A. Mostofi, J. R. Yates, I. Souza, and D. Vanderbilt, Maximally localized Wannier functions: Theory and applications, *Reviews of Modern Physics* **84**, 1419 (2012).
- [52] I. A. Gonoskov, N. Tsatrafyllis, I. K. Kominis, and P. Tzallas, Quantum optical signatures in strong-field laser physics: Infrared photon counting in high-order-harmonic generation, *Scientific Reports* **6**, 32821 (2016).
- [53] N. Tsatrafyllis, I. K. Kominis, I. A. Gonoskov, and P. Tzallas, High-order harmonics measured by the photon statistics of the infrared driving-field exiting the atomic medium, *Nature Communications* **8**, 15170 (2017).
- [54] A. Gorlach, O. Neufeld, N. Rivera, O. Cohen, and I. Kaminer, The quantum-optical nature of high harmonic generation, *Nature Communications* **11**, 4598 (2020).
- [55] N. Rivera and I. Kaminer, Light-matter interactions with photonic quasiparticles, *Nature Reviews Physics* **2**, 538 (2020).
- [56] S. Varró, Quantum Optical Aspects of High-Harmonic Generation, *Photonics* **8**, 269 (2021).
- [57] P. Földi, I. Magashegyi, A. Gombkötő, and S. Varró, Describing High-Order Harmonic Generation Using Quantum Optical Models, *Photonics* **8**, 263 (2021).
- [58] M. Lewenstein, M. F. Ciappina, E. Pisanty, J. Rivera-Dean, P. Stammer, T. Lamprou, and P. Tzallas, Generation of optical Schrödinger cat states in intense laser-matter interactions, *Nature Physics* **17**, 10.1038/s41567-021-01317-w (2021).
- [59] A. Gombkötő, P. Földi, and S. Varró, Quantum-optical description of photon statistics and cross correlations in high-order harmonic generation, *Physical Review A* **104**, 033703 (2021).
- [60] J. Rivera-Dean, P. Stammer, A. S. Maxwell, T. Lamprou, P. Tzallas, M. Lewenstein, and M. F. Ciappina, Light-matter entanglement after above-threshold ionization processes in atoms (2022), arXiv:2208.05245 [physics, physics:quant-ph].
- [61] P. Stammer, J. Rivera-Dean, T. Lamprou, E. Pisanty, M. F. Ciappina, P. Tzallas, and M. Lewenstein, High Photon Number Entangled States and Coherent State Superposition from the Extreme Ultraviolet to the Far Infrared, *Physical Review Letters* **128**, 123603 (2022).
- [62] P. Stammer, J. Rivera-Dean, A. Maxwell, T. Lamprou, A. Ordóñez, M. F. Ciappina, P. Tzallas, and M. Lewenstein, Quantum electrodynamics of ultra-intense laser-matter interactions (2022), arXiv:2206.04308 [physics, physics:quant-ph].
- [63] A. Pizzi, A. Gorlach, N. Rivera, A. Nunnenkamp, and I. Kaminer, Light emission from strongly driven many-body systems (2022), arXiv:2210.03759 [cond-mat, physics:physics, physics:quant-ph].
- [64] P. Stammer, Theory of entanglement and measurement in high harmonic generation (2022), number: arXiv:2203.04354 [physics, physics:quant-ph].
- [65] J. Rivera-Dean, T. Lamprou, E. Pisanty, P. Stammer, A. F. Ordóñez, A. S. Maxwell, M. F. Ciappina

- pina, M. Lewenstein, and P. Tzallas, Strong laser fields and their power to generate controllable high-photon-number coherent-state superpositions, *Physical Review A* **105**, 033714 (2022).
- [66] A. H. Chin, O. G. Calderón, and J. Kono, Extreme Mid-infrared Nonlinear Optics in Semiconductors, *Physical Review Letters* **86**, 3292 (2001).
- [67] This assumption implies that the electron-electron interactions are neglected. There exists, however, a phenomenological way to incorporate them.
- [68] H. Haug and S. W. Koch, Periodic Lattice of Atoms, in *Quantum Theory of the Optical and Electronic Properties of Semiconductors* (World Scientific Publishing Co. Pte. Ltd., 2004) Chap. 3, pp. 41–44.
- [69] W. Kohn, Analytic Properties of Bloch Waves and Wannier Functions, *Physical Review* **115**, 809 (1959).
- [70] I. Vurgaftman, J. R. Meyer, and L. R. Ram-Mohan, Band parameters for III-V compound semiconductors and their alloys, *Journal of Applied Physics* **89**, 5815 (2001).
- [71] U. Özgür, Y. I. Alivov, C. Liu, A. Teke, M. A. Reshchikov, S. Doğan, V. Avrutin, S.-J. Cho, and H. Morkoç, A comprehensive review of ZnO materials and devices, *Journal of Applied Physics* **98**, 041301 (2005).
- [72] A. Schleife, F. Fuchs, C. Rödl, J. Furthmüller, and F. Bechstedt, Band-structure and optical-transition parameters of wurtzite MgO, ZnO, and CdO from quasiparticle calculations, *physica status solidi (b)* **246**, 2150 (2009).
- [73] Q. Yan, P. Rinke, M. Winkelkemper, A. Qteish, D. Bimberg, M. Scheffler, and C. G. Van de Walle, Strain effects and band parameters in MgO, ZnO, and CdO, *Applied Physics Letters* **101**, 152105 (2012).
- [74] C. Gerry and P. Knight, *Introductory Quantum Optics* (Cambridge University Press, Cambridge, UK, 2005).
- [75] M. O. Scully and M. S. Zubairy, *Quantum optics* (Cambridge University Press, Cambridge, 2001).
- [76] In the multielectron scenario, where more than one electron participate in the process, we expect these values to increase. However, we note that in the case of atoms, experimental evidence leads to  $|\delta| \lesssim 1$  when taking into account the HHG effects as well. Thus, we expect this approximation to lead to reasonable predictions in the multielectron case.
- [77] O. Smirnova and M. Ivanov, Multielectron high harmonic generation: Simple man on a complex plane, in *Attosecond and XUV Physics* (John Wiley & Sons, Ltd, 2014) Chap. 7, pp. 201–256.
- [78] J. Schwinger, Casimir energy for dielectrics., Proceedings of the National Academy of Sciences **89**, 4091 (1992).
- [79] G. Vacanti, S. Pugnetti, N. Didier, M. Paternostro, G. M. Palma, R. Fazio, and V. Vedral, Photon Production from the Vacuum Close to the Superradiant Transition: Linking the Dynamical Casimir Effect to the Kibble-Zurek Mechanism, *Physical Review Letters* **108**, 093603 (2012).
- [80] A. Royer, Wigner function as the expectation value of a parity operator, *Physical Review A* **15**, 449 (1977).
- [81] P. van Loock, Optical hybrid approaches to quantum information, *Laser & Photonics Reviews* **5**, 167 (2011).
- [82] L. Amico, R. Fazio, A. Osterloh, and V. Vedral, Entanglement in many-body systems, *Reviews of Modern Physics* **80**, 517 (2008).
- [83] M. A. Nielsen and I. L. Chuang, *Quantum Computation and Quantum Information: 10th Anniversary Edition* (Cambridge University Press, 2010).
- [84] W. Dür, G. Vidal, and J. I. Cirac, Three qubits can be entangled in two inequivalent ways, *Physical Review A* **62**, 062314 (2000).
- [85] S. B. Papp, K. S. Choi, H. Deng, P. Lougovski, S. J. van Enk, and H. J. Kimble, Characterization of Multipartite Entanglement for One Photon Shared Among Four Optical Modes, *Science* **324**, 764 (2009).
- [86] N. Brunner, J. Sharam, and T. Vértesi, Testing the Structure of Multipartite Entanglement with Bell Inequalities, *Physical Review Letters* **108**, 110501 (2012).
- [87] A. Cabello, Bell's theorem with and without inequalities for the three-qubit Greenberger-Horne-Zeilinger and W states, *Physical Review A* **65**, 032108 (2002).
- [88] A. Sen(De), U. Sen, M. Wieśniak, D. Kaszlikowski, and M. Żukowski, Multiqubit W states lead to stronger non-classicality than Greenberger-Horne-Zeilinger states, *Physical Review A* **68**, 062306 (2003).
- [89] B.-S. Shi and A. Tomita, Teleportation of an unknown state by W state, *Physics Letters A* **296**, 161 (2002).
- [90] H.-Y. Dai, P.-X. Chen, and C.-Z. Li, Probabilistic teleportation of an arbitrary two-particle state by two partial three-particle entangled W states, *Journal of Optics B: Quantum and Semiclassical Optics* **6**, 106 (2003).
- [91] V. N. Gorbachev, A. I. Trubillo, A. A. Rodichkina, and A. I. Zhiliba, Can the states of the W-class be suitable for teleportation?, *Physics Letters A* **314**, 267 (2003).
- [92] P. Agrawal and A. Pati, Perfect teleportation and superdense coding with w states, *Physical Review A* **74**, 062320 (2006).
- [93] J. Joo, J. Lee, J. Jang, and Y.-J. Park, Quantum Secure Communication with W States (2002), arXiv:quant-ph/0204003.
- [94] W. Jian, Z. Quan, and T. Chao-Jing, Quantum Secure Communication Scheme with w State, *Communications in Theoretical Physics* **48**, 637 (2007).
- [95] D. Li, X. Xiao-Ming, G. Ya-Jun, and C. Feng, Improvement on Quantum Secure Direct Communication with W State in Noisy Channel, *Communications in Theoretical Physics* **51**, 232 (2009).
- [96] A. Sanpera, R. Tarrach, and G. Vidal, Quantum separability, time reversal and canonical decompositions (1997), arXiv:quant-ph/9707041.
- [97] G. Wang and T.-Y. Du, Quantum decoherence in high-order harmonic generation from solids, *Physical Review A* **103**, 063109 (2021).
- [98] N. W. Ashcroft and N. D. Mermin, Electron Levels in a Periodic Potential: General Properties, in *Solid State Physics* (Cengage Learning, USA, 1976) Chap. 8, pp. 131–150.
- [99] J. Rivera-Dean, P. Stammer, A. S. Maxwell, T. Lamprou, A. F. Ordóñez, E. Pisanty, P. Tzallas, M. Lewenstein, and M. F. Ciappina, Quantum optical analysis of high-harmonic generation in solids within a wannier-block picture, Zenodo (2022).
- [100] P. Virtanen, R. Gommers, T. E. Oliphant, M. Haberland, T. Reddy, D. Cournapeau, E. Burovski, P. Peterson, W. Weckesser, J. Bright, S. J. van der Walt, M. Brett, J. Wilson, K. J. Millman, N. Mayorov, A. R. J. Nelson, E. Jones, R. Kern, E. Larson, C. J. Carey, İ. Polat, Y. Feng, E. W. Moore, J. VanderPlas, D. Laxalde,

- J. Perktold, R. Cimrman, I. Henriksen, E. A. Quintero, C. R. Harris, A. M. Archibald, A. H. Ribeiro, F. Pedregosa, P. van Mulbregt, and SciPy 1.0 Contributors, SciPy 1.0: Fundamental Algorithms for Scientific Computing in Python, *Nat. Meth.* **17**, 261 (2020).
- [101] A. Chacón, D. Kim, W. Zhu, S. P. Kelly, A. Dauphin, E. Pisanty, A. S. Maxwell, A. Picón, M. F. Ciappina, D. E. Kim, C. Ticknor, A. Saxena, and M. Lewenstein, Circular dichroism in higher-order harmonic generation: Heralding topological phases and transitions in Chern insulators, *Physical Review B* **102**, 134115 (2020).

## APPENDIX

### A. Wannier and Bloch states

According to Bloch's theorem, the eigenstates of a single-electron Hamiltonian with a periodic potential, can be written as the product of a plane wave and a function that has the periodicity of the applied potential [98]. In particular, for a one-dimensional system the Bloch functions read

$$\langle x | \phi_{c,k} \rangle = \phi_{m,k}(x) = u_{m,k}(x) e^{ikx}, \quad (\text{A1})$$

where  $m$  is a subscript specifying the band over which the corresponding Bloch wavefunction is defined, and  $k$  is the crystal momentum. These wavefunctions, can be represented as well as

$$\langle x | w_{m,j} \rangle = w_{m,j}(x) = \int_{\text{BZ}} dk \phi_{m,k}(x - x_j) \tilde{w}_m(k), \quad (\text{A2})$$

and which are referred to as Wannier functions. Here,  $\tilde{w}_m(k)$  is a product of a normalization constant and a phase that depends on the crystal momentum  $k$ . However, and as shown in Ref. [69], for a 1D lattice this function is independent of  $k$ . We observe that, unlike the set of Bloch wavefunctions which are completely delocalized in space due to their plane wave nature, Wannier states are defined as a superposition within the Brillouin zone of all possible Bloch states, which leads a localized wavepacket within the real space [51].

#### 1. Computing the matrix element $\langle w_{v,j} | \hat{X} | \phi_{c,k} \rangle$

In order to compute the different quantities we study along the main text, we need to use the previous definitions of Bloch and Wannier states. Of particular importance for our purposes, is the transition matrix element between a Wannier-valence band state and a Bloch-conduction band state, i.e.,  $d_{j,c}(k) = e \langle w_{v,j} | \hat{X} | \phi_{c,k} \rangle$ . First, we introduce the identity in the position representation so that the previous element can be written as

$$\begin{aligned} d_{j,c}(k) &= e \int dx w_{v,j}^*(x) x \phi_{c,k}(x) \\ &= e \tilde{w}_v^* \int dx \int_{\text{BZ}} dk' \phi_{v,k'}^*(x - x_j) x \phi_{c,k}(x). \end{aligned} \quad (\text{A3})$$

Noting that Bloch wavefunctions are periodic, so that for site  $x_j = j\mathbf{a}$ , with  $\mathbf{a}$  the lattice constant, we can write

$$\phi_{c,k}(x - x_j) = \phi_{c,k}(x) e^{-ikx_j}, \quad (\text{A4})$$

and which we can express as

$$\langle w_{v,j} | (\hat{X} - x_j) | \phi_{c,k} \rangle = \langle w_{v,j} | \hat{X} | \phi_{c,k} \rangle, \quad (\text{A5})$$

due to the orthonormality between Wannier and Bloch states. We then have

$$\begin{aligned} d_{j,c}(k) &= e \tilde{w}_v^* \int dx \int_{\text{BZ}} dk' [\phi_{v,k'}^*(x - x_j)] (x - x_j) [\phi_{c,k}(x - x_j)] e^{ikx_j} \\ &= e \tilde{w}_v^* e^{ikx_j} \int_{\text{BZ}} dk' \langle \phi_{v,k'} | \hat{X} | \phi_{c,k} \rangle. \end{aligned} \quad (\text{A6})$$

Finally, we take into account that

$$e \langle \phi_{v,k'} | \hat{X} | \phi_{c,k} \rangle = d_{v,c}(k) \delta(k' - k), \quad (\text{A7})$$

where  $d_{v,c}(k) = e \langle \phi_{v,k} | \hat{X} | \phi_{v,k} \rangle$ , such that we can write

$$d_{j,c}(k) = \tilde{w}_v^* e^{ikx_j} d_{v,c}(k). \quad (\text{A8})$$

## 2. Computing the matrix element $\langle \phi_{v,k} | \hat{X} | \phi_{c,k} \rangle$

From what we have seen above, the transition matrix element between a Wannier-valence band and a Bloch-conduction band state, depends on the transition matrix element between two Bloch states located in the corresponding bands. Hence, we are now interested in computing  $d_{v,c}(k)$ . With that purpose, we take into account that

$$[\hat{X}, \hat{H}_{\text{cr}}] = \frac{i\hbar}{m} \hat{P}_x, \quad (\text{A9})$$

where  $m$  is the electron mass,  $\hat{H}_{\text{cr}}$  the crystal Hamiltonian, and  $\hat{P}_x$  the momentum operator along the  $x$  direction. According to this expression, we can write

$$\langle \phi_{v,k} | \hat{X} | \phi_{c,k} \rangle = \frac{i\hbar}{m} \frac{\langle \phi_{v,k} | \hat{P}_x | \phi_{c,k} \rangle}{\mathcal{E}(k)}, \quad (\text{A10})$$

where we have denoted  $\mathcal{E}(k) = \mathcal{E}_v(k) - \mathcal{E}_c(k)$ . Similarly to what we did before, we now proceed to evaluate the matrix element of the momentum operator  $\hat{P}_x$  by introducing the identity in the position representation, taking into account that

$$\langle x | \hat{P}_x | x' \rangle = -i\hbar \frac{\partial}{\partial x} \delta(x - x'). \quad (\text{A11})$$

This allows us to write

$$\langle \phi_{v,k} | \hat{P}_x | \phi_{c,k} \rangle = -i\hbar \int dx \phi_{v,k}^*(x) \frac{\partial \phi_{c,k}(x)}{\partial x}, \quad (\text{A12})$$

and expanding the Bloch wavefunctions up to the leading term in the  $\mathbf{k} \cdot \mathbf{p}$  theory [68]

$$\phi_{m,k}(x) \simeq e^{ikx} \frac{u_{m,0}(x)}{a^{3/2}}, \quad (\text{A13})$$

such that

$$\frac{\partial \phi_{m,k}(x)}{\partial x} = ik\phi_{m,k}(x) + \frac{e^{ikx}}{a^{3/2}} \frac{\partial u_{m,0}(x)}{\partial x}, \quad (\text{A14})$$

we can write the matrix element of the momentum operator as

$$\langle \phi_{v,k} | \hat{P}_x | \phi_{c,k} \rangle = -\frac{i\hbar}{a^3} \int dx u_{v,0}^* u_{c,0}'(x) \equiv p_{v,c}(0), \quad (\text{A15})$$

where we have taken into account that  $\langle \phi_{v,k} | \phi_{c,k} \rangle = 0$ . With all the above, we get for the initial transition matrix element

$$d_{v,c}(k) = -\frac{i\hbar e}{m} \frac{p_{v,c}(0)}{\mathcal{E}(k)}. \quad (\text{A16})$$

In the bibliography, one can find tabulated values for the so-called Kane parameter  $\mathfrak{E}_{p,i}$ , with  $i \in \{x, y, z\}$ , of different solids, which is related to the element  $p_{v,c}(0)$  by  $\mathfrak{E}_{p,x} = 2p_{v,c}^2(0)$ . Thus, in terms of the Kane parameter, the transition matrix element reads

$$d_{v,c}(k) = -\frac{i\hbar e}{m} \sqrt{\frac{\mathfrak{E}_{p,x}}{2\mathcal{E}^2(k)}}. \quad (\text{A17})$$

## 3. Computing the matrix element $\langle w_{v,j} | \hat{X} | w_{v,j'} \rangle$

Finally, and to conclude with this section, we proceed to compute the matrix element  $\langle w_{v,j} | \hat{X} | w_{v,j'} \rangle$ . In this case, we have in the position representation

$$\begin{aligned} \langle w_{v,j} | \hat{X} | w_{v,j'} \rangle &= \int dx w_{v,j}(x) x w_{v,j'}(x) \\ &= |\tilde{w}_v|^2 \int dx x \int_{\text{BZ}} dk \int_{\text{BZ}} dk' \phi_{v,k}^*(x - x_j) \phi_{v,k}(x - x_{j'}), \end{aligned} \quad (\text{A18})$$

where in the last step we have introduced the definition of Wannier states in terms of the Bloch functions. By taking into account Eq. (A4), we then have

$$\begin{aligned}\langle w_{v,j} | \hat{X} | w_{v,j'} \rangle &= |\tilde{w}_v|^2 \int_{\text{BZ}} dk \int_{\text{BZ}} dk' e^{ikx_j - ik'x_{j'}} \int dx \phi_{v,k}^*(x) x \phi_{v,k}(x) \\ &= i\hbar |\tilde{w}_v|^2 \int_{\text{BZ}} dk \int_{\text{BZ}} dk' e^{ikx_j - ik'x_{j'}} \frac{\partial}{\partial k} \delta(k - k') \\ &= \hbar x_{j'} |\tilde{w}_v|^2 \int_{\text{BZ}} dk e^{ik(x_j - x_{j'})} = x_{j'} \delta_{j,j'}.\end{aligned}\quad (\text{A19})$$

## B. Solving the time-dependent Schrödinger equation

In this appendix section, we introduce the decomposition presented in Eq. (10) into Eq. (9), and proceed to solve it by projecting the equation with respect to a Bloch or a Wannier state, depending on whether we want to study the dynamics of the conduction or valence band, respectively.

### 1. Conditioning to the conduction band

Here, we are interested in studying the dynamics of the conduction band. With that purpose, we project Eq. (9) with respect to a Bloch state  $|\phi_{c,k}\rangle$ , such that we get

$$i\hbar \frac{\partial}{\partial t} (a_c(k, t) |\Phi_c(k, t)\rangle) = \langle \phi_{c,k} | \hat{H}_{\text{cr}} | \Psi'(t) \rangle + eE_{\text{cl}}(t) \langle \phi_{c,k} | \hat{X} | \Psi'(t) \rangle + e\hat{E}(t) \langle \phi_{c,k} | \hat{X} | \Psi'(t) \rangle, \quad (\text{B1})$$

and having in mind that

$$\langle \phi_{c,k} | \hat{H}_{\text{cr}} | \phi_{c,k'} \rangle = \mathcal{E}_c(k) \delta(k - k'), \quad \langle \phi_{c,k} | \hat{X} | \phi_{c,k'} \rangle = i\hbar \frac{\partial}{\partial k} \delta(k - k'), \quad e \langle \phi_{c,k} | \hat{X} | w_{v,j} \rangle = d_{j,c}^*(k), \quad (\text{B2})$$

we can rewrite the previous Schrödinger equation as follows

$$\begin{aligned}i\hbar \frac{\partial}{\partial t} (a_c(k, t) |\Phi_c(k, t)\rangle) &= \mathcal{E}_c(k) a_c(k, t) |\Phi_c(k, t)\rangle + (E_{\text{cl}}(t) + \hat{E}(t)) \sum_j d_{j,c}(k) a_j(t) |\Phi_{v,j}(t)\rangle \\ &\quad + i\hbar e (E_{\text{cl}}(t) + \hat{E}(t)) \frac{\partial}{\partial k} (a_c(k, t) |\Phi_c(k, t)\rangle),\end{aligned}\quad (\text{B3})$$

which has an homogeneous and an inhomogeneous part. Since this kind of differential equations can be written as a linear combination of the solution to the homogeneous equation, and a particular solution to the inhomogeneous, we first consider the former

$$\begin{aligned}i\hbar \frac{\partial}{\partial t} (a_c(k, t) |\Phi_c(k, t)\rangle) &= \mathcal{E}_c(k) a_c(k, t) |\Phi_c(k, t)\rangle + i\hbar e E_{\text{cl}}(t) \frac{\partial}{\partial k} (a_c(k, t) |\Phi_c(k, t)\rangle) \\ &\quad + i\hbar e \hat{E}(t) \frac{\partial}{\partial k} (a_c(k, t) |\Phi_c(k, t)\rangle),\end{aligned}\quad (\text{B4})$$

In the above equation, at the right hand side, we distinguish three different terms. The first one introduces the energy of an electron that is in the conduction band with crystal momentum  $k$ ; the second describes the influence of the average value of the field on the electron's trajectory; finally, the third one characterizes the quantum fluctuations. Moreover, when applying the chain rule to the derivative in this last term, we get two contributions: one that introduces the backaction of the electron's trajectory in the quantum optical state of the field, while the second governs the backaction of the quantum optical perturbations in the semiclassical trajectories. In the following, and in agreement with Ref. [60], we work under the assumption that the electron trajectories do not get affected by the quantum optical fluctuations, such that we omit the last term we have just described. Thus, the Schrödinger equation we are going to study becomes

$$\begin{aligned}i\hbar \frac{\partial}{\partial t} (a_c(k, t) |\Phi_c(k, t)\rangle) &= \mathcal{E}_c(k) a_c(k, t) |\Phi_c(k, t)\rangle + i\hbar e E_{\text{cl}}(t) \frac{\partial}{\partial k} (a_c(k, t) |\Phi_c(k, t)\rangle) \\ &\quad + i\hbar e \hat{E}(t) \left( \frac{\partial a_c(k, t)}{\partial k} \right) |\Phi_c(k, t)\rangle.\end{aligned}\quad (\text{B5})$$

At this point, we consider a change from the crystal momentum frame  $k$  to the canonical momentum  $p = k + \frac{e}{c}A(t)$ , where  $A(t)$  is the field's vector potential given by  $E_{\text{cl}}(t) = (-1/c) \partial A(t)/\partial t$ . We note that the canonical momentum  $p$  is defined in the Brillouin zone shifted by  $A(t)$ , i.e.,  $\tilde{\text{BZ}} = \text{BZ} - A(t)$ . By implementing this change, we can write the above equation in terms of total derivatives with respect to time

$$i\hbar \frac{d}{dt} (a_c(p, t) |\Phi_c(p, t)\rangle) = \mathcal{E}_c(k) a_c(p, t) |\Phi_c(p, t)\rangle + i\hbar e \hat{E}(t) \left( \frac{\partial}{\partial k} a_c(p, t) \right) |\Phi_c(p, t)\rangle, \quad (\text{B6})$$

and which we write as the sum of two contributions

$$\left[ i\hbar \frac{da_c(p, t)}{dt} - \mathcal{E}_c(p) a_c(p, t) \right] |\Phi_c(p, t)\rangle + \left[ i\hbar \frac{d|\Phi_c(p, t)\rangle}{dt} a_c(p, t) - i\hbar e \hat{E}(t) \left( \frac{\partial}{\partial p} a_c(p, t) \right) |\Phi_c(p, t)\rangle \right] = 0. \quad (\text{B7})$$

In order to solve this differential equation, we first look for an  $a_c(p, t)$  that makes the first bracket term equal to zero, i.e., we first solve the following differential equation

$$i\hbar \frac{da_c(p, t)}{dt} - \mathcal{E}_c(p) a_c(p, t) = 0, \quad (\text{B8})$$

whose solution we easily find to be

$$a_c(p, t) = a_c(p, t_0) \exp \left[ -\frac{i}{\hbar} \int_{t_0}^t d\tau \mathcal{E}_c \left( p - \frac{e}{c} A(\tau) \right) \right] = a_c(p, t_0) e^{-\frac{i}{\hbar} S(p, t, t_0)}, \quad (\text{B9})$$

and whose partial derivative with respect to  $p$  is given by

$$i\hbar \frac{\partial a_c(p, t)}{\partial p} = a_c(p, t) \Delta r(p, t, t_0), \quad (\text{B10})$$

where  $\Delta r(p, t, t_0)$  is the displacement performed by the electron within the conduction band from  $t_0$  to  $t$ , and which is given by

$$\Delta r(p, t, t_0) = \int_{t_0}^t d\tau \frac{\partial}{\partial p} \mathcal{E}_c \left( p - \frac{e}{c} A(\tau) \right). \quad (\text{B11})$$

We now introduce this result in Eq. (B7) to find

$$i\hbar \frac{d|\Phi_c(p, t)\rangle}{dt} = e \hat{E}(t) \Delta r(p, t, t_0) |\Phi_c(p, t)\rangle, \quad (\text{B12})$$

whose right hand side is given as a linear combination of creation and annihilation operators acting on all field modes, but where we do not have any sort of interaction between the field modes. Thus, a solution to this differential equation can be written as [62, 65]

$$|\Phi_c(p, t)\rangle = \hat{\mathbf{D}}(\delta(p, t, t_0)) |\Phi_c(p, t_0)\rangle = \prod_{\mathbf{k}} e^{i\varphi_{\mathbf{k}}} \hat{D}(\delta_{\mathbf{k}}(p, t, t_0)) |\Phi_c(p, t_0)\rangle, \quad (\text{B13})$$

where  $\varphi_{\mathbf{k}}(p, t)$  is a phase prefactor appearing due to the introduction of the Baker-Campbell-Hausdorff (BCH) formula [74, 75], and where  $\delta_{\mathbf{k}}(p, t, t_0)$  is given by

$$\delta_{\mathbf{k}}(p, t, t_0) = -\frac{e}{\hbar} \sqrt{\frac{\hbar c |\mathbf{k}|}{2\epsilon_0 V}} \int_{t_0}^t d\tau \Delta r(p, \tau, t_0) e^{i\omega_{\mathbf{k}} \tau}. \quad (\text{B14})$$

Thus, from all the above we conclude that the solution to the homogeneous equation given in Eq. (B7) can be written as

$$(a_c(p, t) |\Phi_c(p, t)\rangle)_{\text{hom}} = e^{-\frac{i}{\hbar} S(p, t, t_0)} \hat{\mathbf{D}}(\delta(p, t, t_0)) a_c(p, t_0) |\Phi_c(p, t_0)\rangle, \quad (\text{B15})$$

such that the solution to the inhomogeneous equation, under the considered approximations and with the corresponding initial state, reads

$$a_c(p, t) |\Phi_c(p, t)\rangle = -\frac{i}{\hbar} \sum_j \int_{t_0}^t dt_1 e^{-i\frac{i}{\hbar} S(p, t, t_1)} \hat{\mathbf{D}}(\delta(p, t, t_1)) (E_{\text{cl}}(t_1) + \hat{E}(t_1)) d_{j,c}^*(p - \frac{e}{c} A(t_1)) a_j(t_1) |\Phi_{v,j}(t_1)\rangle. \quad (\text{B16})$$

## 2. Conditioning to the valence band

After studying the dynamics in the conduction band, we now turn our attention to the analysis of the valence band dynamics. With that purpose, we project Eq. (9) with respect to a Wannier state  $|w_{v,j}\rangle$  to obtain

$$i\hbar \frac{\partial}{\partial t} (a_j(t) |\Phi_{v,j}(t)\rangle) = \langle w_{v,j} | H_{\text{cr}} | \Psi'(t) \rangle + e(E_{\text{cl}}(t) + \hat{E}(t)) \langle w_{v,j} | \hat{X} | \Psi'(t) \rangle. \quad (\text{B17})$$

In this manuscript, we work under the tight-binding approximation and consider that the electron can only hop to its nearest-neighboring sites. Thus, we write

$$\langle w_{v,j} | H_{\text{cr}} | w_{v,j'} \rangle = -I_v \delta_{|j-j'|,1}, \quad (\text{B18})$$

where  $I_v < 0$  is the hopping parameter in the valence band. Furthermore, if we denote

$$e \langle w_{v,j} | \hat{X} | w_{v,j'} \rangle = d_{j,j'}, \quad (\text{B19})$$

then we can expand the previous Schrödinger equation as

$$\begin{aligned} i\hbar \frac{\partial}{\partial t} (a_j(t) |\Phi_{v,j}(t)\rangle) &= -I_v a_{j-1}(t) |\Phi_{v,j-1}(t)\rangle - I_v a_{j+1}(t) |\Phi_{v,j+1}(t)\rangle \\ &\quad + (E_{\text{cl}}(t) + \hat{E}(t)) \left( \sum_{j'} d_{j,j'} a_{v,j'}(t) |\Phi_{v,j}(t)\rangle + \int_{\text{BZ}} dk d_{j,c}(k) a_c(k,t) |\Phi_c(k,t)\rangle \right). \end{aligned} \quad (\text{B20})$$

Note that, in all the analysis we have presented thus far, both interband and intraband transitions have been considered. By introducing the relations derived in Appendix A, we can rewrite the above equation as

$$\begin{aligned} i\hbar \frac{\partial}{\partial t} (a_j(t) |\Phi_{v,j}(t)\rangle) &= -I_v a_{j-1}(t) |\Phi_{v,j-1}(t)\rangle - I_v a_{j+1}(t) |\Phi_{v,j+1}(t)\rangle \\ &\quad + (E_{\text{cl}}(t) + \hat{E}(t)) \left( e x_j a_{v,j}(t) |\Phi_{v,j}(t)\rangle + \int_{\text{BZ}} dk d_{j,c}(k) a_c(k,t) |\Phi_c(k,t)\rangle \right). \end{aligned} \quad (\text{B21})$$

In the equation above, the second term of the right hand side has two contributions regarding the electron dynamics: one coming from the electron oscillations in the valence band, and another that accounts for the transitions to the valence band. We note that the latter is already proportional to  $eE_0 \sim 10^{-3}$  a.u., with  $E_0$  the field's amplitude, which makes the whole term to be proportional to  $(eE_0)^2$ . Therefore, using this quantity as a perturbation parameter, we then write

$$a_j(t) |\Phi_{v,j}(t)\rangle = a_j^{(0)} |\Phi_{v,j}^{(0)}(t)\rangle + a_j^{(1)} |\Phi_{v,j}^{(1)}(t)\rangle, \quad (\text{B22})$$

where the superscript represents the perturbation order. We now proceed to evaluate each of the perturbation orders separately.

### a. Analysis of the zeroth order term

The differential equation governing the dynamics of the zeroth order term is given by

$$i\hbar \frac{\partial}{\partial t} (a_j^{(0)}(t) |\Phi_{v,j}^{(0)}(t)\rangle) = -I_v a_{j-1}^{(0)}(t) |\Phi_{v,j-1}^{(0)}(t)\rangle - I_v a_{j+1}^{(0)}(t) |\Phi_{v,j+1}^{(0)}(t)\rangle + e(E_{\text{cl}}(t) + \hat{E}(t)) x_j a_{v,j}^{(0)}(t) |\Phi_{v,j}^{(0)}(t)\rangle, \quad (\text{B23})$$

and, in order to solve it, we perform a discrete Fourier transform over the site label  $j$ , by multiplying the whole equation by  $e^{-iqj}$  and summing over all the sites  $j$ . Thus, if we define

$$a_q(t) |\Phi_{v,q}(t)\rangle = \sum_j a_j(t) |\phi_{v,j}(t)\rangle e^{-iqj}, \quad (\text{B24})$$

we then have the following:

- for the time-derivative at the left hand side, we can write

$$\sum_j \frac{\partial}{\partial t} (a_j(t) |\Phi_{v,j}(t)\rangle) e^{-iqj} = \frac{\partial}{\partial t} \left( \sum_j a_j(t) |\Phi_{v,j}(t)\rangle e^{-iqj} \right) = \frac{\partial}{\partial t} (a_q(t) |\Phi_{v,q}(t)\rangle); \quad (\text{B25})$$

- for the hopping term at the left hand side, we find

$$\begin{aligned} -I_v \sum_j (a_{j-1}(t) |\Phi_{v,j-1}(t)\rangle e^{-iqj} + a_{j+1}(t) |\Phi_{v,j+1}(t)\rangle e^{-iqj}) &= -I_v (a_q(t) |\Phi_{v,q}(t)\rangle e^{iq} + a_q(t) |\Phi_{v,q}(t)\rangle e^{-iq}) \\ &= -2I_v \cos(q) a_q(t) |\Phi_{v,q}(t)\rangle; \end{aligned} \quad (\text{B26})$$

- finally, for the last term involving the interaction with the electromagnetic field, we get

$$\sum_j x_j a_j(t) |\Phi_{v,j}(t)\rangle e^{-iqj} = i\mathbf{a} \sum_j (-ij) a_j(t) |\Phi_{v,j}(t)\rangle e^{-iqj} = i\mathbf{a} \frac{\partial}{\partial q} (a_q(t) |\Phi_{v,q}(t)\rangle). \quad (\text{B27})$$

With all the above, the Schrödinger equation for the zeroth order term in the reciprocal space reads

$$i\hbar \frac{\partial}{\partial t} (a_q^{(0)}(t) |\Phi_{v,q}^{(0)}(t)\rangle) = -2I_v \cos(q) a_q^{(0)}(t) |\Phi_{v,q}^{(0)}(t)\rangle + i\mathbf{a} (E_{\text{cl}}(t) + \hat{E}(t)) \frac{\partial}{\partial q} (a_q^{(0)}(t) |\Phi_{v,q}^{(0)}(t)\rangle), \quad (\text{B28})$$

which has a similar form to that obtained for the conduction band analysis, although within a different context. In particular, the first term at the right hand side corresponds to the energy associated to an electron that is located in the  $q$ th site of the reciprocal lattice, while the second term introduces the effects of the average field on the trajectories that the electron can follow in the reciprocal space, together with the associated quantum optical fluctuations. Introducing here a similar approximation to that of the conduction band Schrödinger equation regarding the influence of the quantum fluctuations on the semiclassical trajectories, we approximate the previous differential equation by

$$i\hbar \frac{\partial}{\partial t} (a_q^{(0)}(t) |\Phi_{v,q}^{(0)}(t)\rangle) = -2I_v \cos(q) a_q^{(0)}(t) |\Phi_{v,q}^{(0)}(t)\rangle + i\mathbf{a} E_{\text{cl}}(t) \frac{\partial}{\partial q} (a_q^{(0)}(t) |\Phi_{v,q}^{(0)}(t)\rangle) + i\mathbf{a} \hat{E}(t) \left( \frac{\partial}{\partial q} a_q^{(0)}(t) \right) |\Phi_{v,q}^{(0)}(t)\rangle. \quad (\text{B29})$$

We now move to a displaced frame of reference by performing the change of variables  $q = \tilde{q} - \frac{e\mathbf{a}}{\hbar c} A(t)$ , with  $A(t)$  the field's vector potential, which allows us to define total derivatives with respect to time. With all the above, we can write our differential equation as a sum of two contributions

$$\left[ i\hbar \frac{da_{\tilde{q}}^{(0)}(t)}{dt} + 2I_v \cos\left(\tilde{q} - \frac{e\mathbf{a}}{\hbar c} A(t)\right) a_{\tilde{q}}^{(0)}(t) \right] |\Phi_{v,\tilde{q}}^{(0)}(t)\rangle + \left[ i\hbar \frac{d|\Phi_{v,\tilde{q}}^{(0)}(t)\rangle}{dt} a_{\tilde{q}}^{(0)}(t) - i\mathbf{a} \hat{E}(t) \left( \frac{\partial a_{\tilde{q}}^{(0)}(t)}{\partial \tilde{q}} \right) |\Phi_{v,\tilde{q}}^{(0)}(t)\rangle \right] = 0, \quad (\text{B30})$$

which we proceed to solve similarly as to the one obtained in the conduction band analysis: we first look for an  $a_{\tilde{q}}^{(0)}(t)$  that makes the first term between brackets equal to zero, and in second place we introduce the obtained result in the differential equation. Thus, we first study the following differential equation

$$i\hbar \frac{da_{\tilde{q}}^{(0)}(t)}{dt} + 2I_v \cos\left(\tilde{q} - \frac{e\mathbf{a}}{\hbar c} A(t)\right) a_{\tilde{q}}^{(0)}(t) = 0, \quad (\text{B31})$$

whose solution we easily find to be

$$a_{\tilde{q}}^{(0)}(t) = a_{\tilde{q}}^{(0)}(t_0) \exp\left[\frac{i}{\hbar} 2I_v \int_{t_0}^t d\tau \cos\left(\tilde{q} - \frac{e\mathbf{a}}{\hbar c} A(\tau)\right)\right] = a_{\tilde{q}}^{(0)}(t_0) e^{\frac{i}{\hbar} 2\tilde{S}(\tilde{q}, t, t_0)}, \quad (\text{B32})$$

and whose partial derivative with respect to  $\tilde{q}$  is given by

$$\frac{\partial a_{\tilde{q}}^{(0)}(t)}{\partial \tilde{q}} = -\frac{i}{\hbar} 2I_v \left( \int_{t_0}^t d\tau \sin\left(\tilde{q} - \frac{e\mathbf{a}}{\hbar c} A(\tau)\right) \right) a_{\tilde{q}}^{(0)}(t). \quad (\text{B33})$$

We remark that the equation presented in Eq. (B31) describes the propagation of the electron in the reciprocal lattice under the influence of an electromagnetic field. Therefore, and similarly to what we got in the conduction band

analysis, the electron acquires a phase which depends on the energy that it has acquired during its displacement, and whose derivative with respect to  $\tilde{q}$  leads to the total displacement performed in the reciprocal space, i.e.

$$\Delta\tilde{r}(\tilde{q}, t, t_0) = \frac{I_v}{\hbar} \int_{t_0}^t d\tau \sin\left(\tilde{q} - \frac{e\mathbf{a}}{\hbar c} A(\tau)\right). \quad (\text{B34})$$

Introducing the above results in Eq. (B30), we get the following differential equation describing the quantum optical behavior

$$i\hbar \frac{d|\Phi_{v,\tilde{q}}^{(0)}(t)\rangle}{dt} - 2\frac{e\mathbf{a}}{\hbar} \Delta\tilde{r} \hat{E}(t)(\tilde{q}, t, t_0) |\Phi_{v,\tilde{q}}^{(0)}(t)\rangle = 0, \quad (\text{B35})$$

which is a linear combination of creation and annihilation operators, that can be solved by means of

$$|\Phi_{v,\tilde{q}}^{(0)}(t)\rangle = \hat{\mathbf{D}}(\tilde{\delta}(\tilde{q}, t, t_0)) |\Phi_{v,\tilde{q}}(t_0)\rangle = \prod_{\mathbf{k}} e^{\varphi_{\mathbf{k}}(\tilde{q}, t)} D(\tilde{\delta}_{\mathbf{k}}(\tilde{q}, t, t_0)) |\Phi_{v,\tilde{q}}(t_0)\rangle, \quad (\text{B36})$$

where  $\varphi_{\mathbf{k}}(\tilde{q}, t)$  is the corresponding BCH prefactor, and where  $\tilde{\delta}_{\mathbf{k}}(\tilde{q}, t, t_0)$  is given by

$$\tilde{\delta}_{\mathbf{k}}(\tilde{q}, t, t_0) = -2\frac{e\mathbf{a}}{\hbar} \sqrt{\frac{\hbar c|\mathbf{k}|}{2\epsilon_0 V}} \int_{t_0}^t d\tau \Delta\tilde{r}(\tilde{q}, \tau, t_0) e^{i\omega_{\mathbf{k}}\tau}. \quad (\text{B37})$$

Thus, in the reciprocal space, the solution to the zeroth order term part of the differential equation is given by

$$a_{\tilde{q}}^{(0)}(t) |\Phi_{v,\tilde{q}}^{(0)}(t)\rangle = e^{\frac{i}{\hbar} 2\tilde{S}(\tilde{q}, t, t_0)} \hat{\mathbf{D}}(\tilde{\delta}(\tilde{q}, t, t_0)) a_{\tilde{q}}(t_0) |\Phi_{v,\tilde{q}}^{(0)}(t_0)\rangle, \quad (\text{B38})$$

and we can transform back to the real space frame by doing the inverse Fourier transform, i.e.

$$a_j^{(0)}(t) |\Phi_{v,j}^{(0)}(t)\rangle = \sum_q e^{iqj} a_q^{(0)}(t) |\Phi_{v,q}^{(0)}(t)\rangle, \quad (\text{B39})$$

such that, having in mind that the initial condition in reciprocal space can be written as

$$a_q^{(0)}(t) |\Phi_{v,q}^{(0)}(t)\rangle = e^{-iqj_0} \bigotimes_{\mathbf{k}} |0_{\mathbf{k}}\rangle, \quad (\text{B40})$$

we get that the solution to the zeroth order part of the differential equation is given by

$$a_j^{(0)}(t) |\Phi_{v,j}^{(0)}(t)\rangle = \sum_q e^{iq(j-j_0)} e^{\frac{i}{\hbar} 2\tilde{S}(\tilde{q}, t, t_0)} \hat{\mathbf{D}}(\tilde{\delta}(q + \frac{e\mathbf{a}}{\hbar c} A(t), t, t_0) \bigotimes_{\mathbf{k}} |0_{\mathbf{k}}\rangle). \quad (\text{B41})$$

### b. Analysis of the first order term

We now focus on the characterization of the first order perturbation theory equation, which is given by

$$i\hbar \frac{\partial}{\partial t} \left( a_j^{(1)}(t) |\Phi_{v,j}^{(1)}(t)\rangle \right) = -I_v a_{j-1}^{(1)}(t) |\Phi_{v,j-1}^{(1)}(t)\rangle - I_v a_{j+1}^{(1)}(t) |\Phi_{v,j+1}^{(1)}(t)\rangle \\ + (E_{\text{cl}}(t) + \hat{E}(t)) \left( d_{j,j} a_{v,j}^{(1)}(t) |\Phi_{v,j}^{(1)}(t)\rangle + \int_{\text{BZ}} dk d_{j,c}(k) a_c(k, t) |\Phi_c(k, t)\rangle \right), \quad (\text{B42})$$

and by performing a discrete Fourier transform, similarly to what we did with the zeroth order term, we get

$$i\hbar \frac{\partial}{\partial t} \left( a_q^{(1)}(t) |\Phi_{v,q}^{(1)}(t)\rangle \right) = -2\frac{I_v}{\hbar} \cos(q) a_q^{(1)}(t) |\Phi_{v,q}^{(1)}(t)\rangle + ie\mathbf{a} (\hat{E}(t) + E_{\text{cl}}(t)) \frac{\partial}{\partial q} \left( a_q^{(1)}(t) |\Phi_{v,q}^{(1)}(t)\rangle \right) \\ + (\hat{E}(t) + E_{\text{cl}}(t)) \sum_j e^{-iqj} \int_{\text{BZ}} dk d_{j,c}(k) a_c(k, t) |\Phi_c(k, t)\rangle, \quad (\text{B43})$$

where we distinguish between an homogeneous and an inhomogeneous part. The homogeneous part of the equation essentially corresponds to the zeroth order term we studied before prior to the introduction of some approximations. Thus, by taking them into account as well as the initial condition, we get that the solution to this differential equation is given by

$$\begin{aligned} a_j^{(1)}(t) \left| \Phi_{v,j}^{(1)}(t) \right\rangle = & \frac{1}{\hbar^2} \sum_{q,j',j''} \int_{t_0}^t dt_2 \int_{\text{BZ}} dp \int_{t_0}^{t_2} dt_1 e^{iq(j-j')} e^{2\frac{i}{\hbar}\tilde{S}(q+\frac{e\mathbf{a}}{\hbar c}A(t),t,t_2)} \mathbf{D}(\tilde{\boldsymbol{\delta}}(q-\frac{e\mathbf{a}}{\hbar c}A(t),t,t_2)) (\hat{E}(t_2) + E_{\text{cl}}(t_2)) \\ & \times d_{j',c} \left( p - \frac{e}{c} A(t_2) \right) e^{-\frac{i}{\hbar}S(p,t_2,t_1)} \hat{\mathbf{D}}(\boldsymbol{\delta}(p,t_2,t_1)) (\hat{E}(t_1) + E_{\text{cl}}(t_1)) d_{j'',c}^* \left( p - \frac{e}{c} A(t_1) \right) a_{j''}^{(0)}(t_1) \left| \Phi_{v,j''}^{(0)}(t_1) \right\rangle, \end{aligned} \quad (\text{B44})$$

where we have further undone the discrete Fourier transform.

### C. Numerical analysis

Most of the numerical effort has been put in the computation of the probability amplitudes shown in Eqs. (37) and (38). In particular, the majority of the computation time was spent in calculating the triple integration that appear in these equations. Here, the implementation we have used is done in Python, and can be found in Ref. [99]. We now present the expression of the integrands as we have implemented them numerically, and discuss how the integrals were performed.

#### 1. Implementation of the probability amplitude in Eq. (37)

As mentioned in the text, Eq. (37) corresponds to the probability amplitude of a process where a photon of frequency  $\omega_{\mathbf{k}}$  is generated at the recombination time  $t_1$ . In order to implement this expression numerically, we first write the transition matrix elements  $d_{j,c}(k)$  as

$$d_{j,c}(k) = \tilde{w}_v^* e^{ikx_j} d_{v,c}, \quad (\text{C1})$$

according to what we discussed in Appendix A. However, we have considered a further approximation, and is to neglect the dependence with the crystal momentum  $k$  in  $d_{v,c}$ , following [23] (see the Supplementary Material of the paper), by setting  $k = 0$ . In this case, the Kane parameter lies in the range  $\mathfrak{E}_{p,x} = 0.248 \rightarrow 0.355$ . In our numerical implementation, we set it to 0.3.

Thus, under the above approximation, Eq. (37) reads (omitting the  $g(\mathbf{k})$  dependence)

$$\mathcal{P}^{(1)}(j, 1_{\mathbf{k}}, t) = \sum_{j'} |\tilde{w}_v|^2 |d_{vc}|^2 \int_{t_0}^t dt_2 \int_{\text{BZ}} dp \int_{t_0}^{t_2} dt_1 e^{i\omega_{\mathbf{k}} t_2} e^{i(p-\frac{e}{c}A(t_2))x_j} e^{-\frac{i}{\hbar}S(p,t_2,t_1)} E_{\text{cl}}(t_1) e^{-i(p-\frac{e}{c}A(t_1))x_j} a_{j'}^{(0)}(t_1), \quad (\text{C2})$$

where we have that

$$S(p, t_1, t_2) = \int_{t_1}^{t_2} d\tau \mathcal{E}_c \left( p - \frac{e}{c} A(\tau) \right) = \int_{t_1}^{t_2} d\tau \left[ \mathcal{E}'_c - 2I_c \cos \left( \left( p - \frac{e}{c} A(\tau) \right) \mathbf{a} \right) \right], \quad (\text{C3})$$

and for the probability amplitude of an electron being in the Wannier site  $j$  of the valence band

$$a_j(t) = \sum_q e^{iq(j'-j_0)} \exp \left[ \frac{i}{\hbar} 2I_v \int_{t_0}^t d\tau \cos \left( \tilde{q} - \frac{e\mathbf{a}}{\hbar c} A(\tau) \right) \right]. \quad (\text{C4})$$

In all our analysis, we consider the vector potential to have a sinusoidal squared envelope, i.e., we work with

$$A(t) = A_0 \sin^2 \left( \frac{\omega_{\mathbf{k}_L}}{2n_{\text{cyc}}} t \right) \sin(\omega t), \quad (\text{C5})$$

where  $n_{\text{cyc}}$  represents the number of cycles. Thus, one of the main problems in computing Eqs. (C3) and (C4) is that there is no trivial exact analytical expression for the integral of the cosine function with the vector potential inside. A clear exception is the case of a monochromatic field, for which these integrals can be written as an expansion in terms of Bessel functions.

Thus, with the aim of writing an analytical expression for these integrals, we first expand the corresponding sinusoidal function as (we use here the integral in Eq. (C3) without loss of generality)

$$\begin{aligned} \int_{t_1}^{t_2} d\tau \cos\left(p\alpha - \frac{e\alpha}{c} A(\tau)\right) &= \cos(p\alpha) \int_{t_1}^{t_2} d\tau \cos\left(\frac{e\alpha}{c} A(\tau)\right) + \sin(p\alpha) \int_{t_1}^{t_2} d\tau \sin\left(\frac{e\alpha}{c} A(\tau)\right) \\ &= \cos(p\alpha) f_1(t_2, t_1) - \sin(p\alpha) f_2(t_2, t_1), \end{aligned} \quad (\text{C6})$$

where we have defined

$$\begin{aligned} f_1(t_2, t_1) &= \int_{t_1}^{t_2} d\tau \cos\left(\frac{e\alpha}{c} A(\tau)\right), \\ f_2(t_2, t_1) &= \int_{t_1}^{t_2} d\tau \sin\left(\frac{e\alpha}{c} A(\tau)\right), \end{aligned} \quad (\text{C7})$$

and we now expand both integrands in Taylor series up to fifth order, which provides a good convergence for the range of values  $A(t)$  can have. Thus, we work with

$$\begin{aligned} f_1(t_2, t_1) &\approx \int_{t_1}^{t_2} d\tau \left(1 - \frac{(\frac{e\alpha}{c} A(\tau))^2}{2!} + \frac{(\frac{e\alpha}{c} A(\tau))^4}{4!}\right), \\ f_2(t_2, t_1) &\approx \int_{t_1}^{t_2} d\tau \left(\frac{e\alpha}{c} A(\tau) - \frac{(\frac{e\alpha}{c} A(\tau))^3}{3!} + \frac{(\frac{e\alpha}{c} A(\tau))^5}{5!}\right). \end{aligned} \quad (\text{C8})$$

Another approximation we did is to limit the values of  $q$  appearing in Eq. (C4) to just a few. Specifically, we set  $q \in [-100, 100]$ , which leads to good convergence. We have to note here that smaller ranges already lead to good convergence, but we went further beyond into that limit to be safe. However, in our implementation this does not impose an important bottleneck since the calculation of  $a_{j'}(t)$  is performed in a vectorized manner.

With all the above, the triple integration in Eq. (C2) was done in two steps:

1. In the first step, we fix  $j$  and compute the integrals for momentum and the excitation time  $t_1$ . We do this for each value of  $j'$  separately, where for the  $\Gamma - A$  band of ZnO we can take the first fifteen values of  $j'$  to get good convergence. These integrals have been performed simultaneously by using the `nquad` function of the `Scipy` Python package [100]. For each value of  $j'$ , the integral was evaluated in a single 2 GHz-CPU core, and the same process has been performed in parallel for four different values of  $j'$  (each in a CPU core). Each of these single evaluations take around 4 hours in the employed machine, and have been done for three different values of  $j$ .
2. In the second step, once all the integrals have already been computed for three different values of  $j$  and fifteen different values of  $j'$ , we sum all the results up and perform an interpolation in time of the obtained function, using the `interp1d` function of the `Scipy` package. Then, we perform the last integral which corresponds to a Fourier transform by using the `quad` function of the aforementioned Python package. This approach leads to Fig. (3) (a) in the main text. This last computation has been performed in a Macbook Air M1 (2020) with 8 CPU cores, considering a total of 150 frequencies, and takes around 1 minute.

## 2. Implementation of the probability amplitude in Eq. (38)

In this case, Eq. (38) represents the probability amplitude of a process where a photon of frequency  $\omega_k$  is generated at the ionization time  $t_2$ , due to vacuum fluctuations. By using Eq. (C1), we can write this probability amplitude as

$$\mathcal{P}^{(2)}(j, 1_k, t) = \sum_{j'} |\tilde{w}_v|^2 |d_{vc}|^2 \int_{t_0}^t dt_2 \int_{BZ} dp \int_{t_0}^{t_2} dt_1 E_{cl}(t_2) e^{i(p - \frac{e}{c} A(t_2))x_j} e^{-\frac{i}{\hbar} S(p, t_2, t_1)} e^{i\omega_k t_1} e^{-i(p - \frac{e}{c} A(t_1))x_j} a_{j'}^{(0)}(t_1). \quad (\text{C9})$$

The main problem regarding the evaluation of these integrals is that, in general, we are interested on how does this quantity change for different frequency terms. This implies changing the frequency  $\omega_k$  depending on the particular case we are interested in. While in Eq. (C2) the associated integral appears as the last one, which allows us to first compute the two inner integrals (either numerically, via the saddle-point approximation or an hybrid approach) and compute the last one using an interpolated approach, in the present case it appears as the inner one. Thus, in order

to follow a similar approach to the one we have been using, we perform a change in the ordering of the integration variables  $t_2$  and  $t_1$ . For this, we note that integrals over  $p$  and  $t_1$  are independent and therefore commute.

According to the integration limits,  $t_2 \in [t_0, T]$ , where  $T$  in our case is the end of the pulse. On the other hand, for the other time integration variable we have  $t_1 \in [t_0, t_2]$ . Having in mind that the integrand is well-behaved, we can swap these two integrals by simply changing the integration limits in each of them properly. In particular, we would have

$$t_1 \in [t_0, T] \text{ and } t_2 \in [t_2, T], \quad (\text{C10})$$

and our integral can be written as

$$\mathcal{P}^{(2)}(j, 1_{\mathbf{k}}, t) = \sum_{j'} |\tilde{w}_v|^2 |d_{vc}|^2 \int_{t_0}^T dt_1 e^{i\omega_{\mathbf{k}} t_1} \int_{t_1}^T dt_2 \int_{\text{BZ}} dp E_{\text{cl}}(t_2) e^{i(p - \frac{e}{c} A(t_2))x_j} e^{-\frac{i}{\hbar} S(p, t_2, t_1)} e^{-i(p - \frac{e}{c} A(t_1))x_j} a_{j'}^{(0)}(t_1). \quad (\text{C11})$$

The way we evaluate these integrals is rather similar to the one presented in the previous subsection. However, instead of using the `nquad` function for computing the first two integrals, we use instead a trapezoidal technique for computing the integral in momentum, while for the one over the recombination time  $t_2$  we employed the `quad` function. The reason of this change is that `nquad` does only admit integration limits which are fixed, and in this case the integration limits of the momentum integral depend on the recombination time via the dependence in time of the shifted Brillouin zone.

### 3. Evaluation of the harmonic spectrum

Finally, the evaluation of the semiclassical spectrum can be performed straightforwardly with the data obtained when computing the previous two integrals. According to Ref. [27], the time-dependent dipole moment can be written as

$$d(t) \propto \sum_{j, j'} |\tilde{w}_v|^2 |d_{vc}|^2 \int_{t_0}^T dt_1 e^{i\omega_{\mathbf{k}} t_1} \int_{t_1}^T dt_2 \int_{\text{BZ}} dp (a_{j'}^{(0)}(t_2))^* E_{\text{cl}}(t_2) e^{i(p - \frac{e}{c} A(t_2))x_j} e^{-\frac{i}{\hbar} S(p, t_2, t_1)} e^{-i(p - \frac{e}{c} A(t_1))x_j} a_{j'}^{(0)}(t_1) + \text{c.c.}, \quad (\text{C12})$$

where the first two integrals are the ones computed in Eq. (C2). Thus, the only difference with respect to the calculation of  $\mathcal{P}^{(1)}(j, 1_{\mathbf{k}}, t)$  is in how the second step of the integrals computation is performed, since now there is an extra  $(a_{j'}^{(0)}(t_2))^*$  dependence.

### D. Evaluating the action of the electric field operators acting at different times

As presented in the main text, the HHG component of the state can be written as

$$|\Psi_{\text{HHG}}(t)\rangle \approx \sum_{j, j'} \int_{t_0}^t dt_2 \int_{\text{BZ}} dp \int_{t_0}^{t_2} dt_1 \hat{E}(t_2) d_{j,c} \left( p - \frac{e}{c} A(t_2) \right) e^{-\frac{i}{\hbar} S(p, t_2, t_1)} \times \hat{E}(t_1) d_{j',c}^* \left( p - \frac{e}{c} A(t_1) \right) a_{j'}^{(0)}(t_1) |\alpha\rangle \bigotimes_{\mathbf{k} \in \text{HH}} |0_{\mathbf{k}}\rangle |w_{v,j}\rangle, \quad (\text{D1})$$

where we have the evaluation of two electric field operators acting at two different times, in particular at the excitation time  $t_1$  and at the recombination time  $t_2$ . Given the expression of the electric field operator in Eq. (7), in our case we have to evaluate

$$\begin{aligned} \hat{E}(t_2) \hat{E}(t_1) &= - \sum_{\mathbf{k}, \mathbf{k}'} \hat{E}_{\mathbf{k}}(t_2) \hat{E}_{\mathbf{k}'}(t_1) \\ &= - \sum_{\mathbf{k}, \mathbf{k}'} g(\mathbf{k}) g(\mathbf{k}') (\hat{a}_{\mathbf{k}}^\dagger e^{i\omega_{\mathbf{k}} t_2} - \hat{a}_{\mathbf{k}} e^{-i\omega_{\mathbf{k}} t_2}) (\hat{a}_{\mathbf{k}'}^\dagger e^{i\omega_{\mathbf{k}'} t_1} - \hat{a}_{\mathbf{k}'} e^{-i\omega_{\mathbf{k}'} t_1}), \end{aligned} \quad (\text{D2})$$

over the initial quantum optical state of the system. Here, we have defined  $g(\mathbf{k}) = \sqrt{\hbar c |\mathbf{k}| / (2\epsilon_0 V)}$ . In the following, we proceed to study how all possible combinations of the form  $\hat{E}_{\mathbf{k}}(t_2) \hat{E}_{\mathbf{k}'}(t_1)$  affect the initial quantum optical state of the system.

### 1. Fundamental-fundamental term

Here, we are going to evaluate the action of  $\hat{E}_{\mathbf{k}_L}(t_2)\hat{E}_{\mathbf{k}_L}(t_1)$  over the initial coherent state of our system  $|\alpha\rangle$ . In order to do so, we take into account the following property of the displacement operator

$$D^\dagger(\alpha)\hat{E}_{\mathbf{k}_L}(t)D(\alpha) = E_{\text{cl}}(t) + \hat{E}_{\mathbf{k}_L}(t), \quad (\text{D3})$$

such that its action over  $|\alpha\rangle$  leads to

$$\begin{aligned} \hat{E}_{\mathbf{k}_L}(t_2)\hat{E}_{\mathbf{k}_L}(t_1)|\alpha\rangle|\{0\}_{\mathbf{k}\in\text{HH}}\rangle &= D(\alpha)(E_{\text{cl}}(t_2) + \hat{E}_{\mathbf{k}_L}(t_2))(E_{\text{cl}}(t_1) + \hat{E}_{\mathbf{k}_L}(t_1))|\bar{0}\rangle \\ &= (E_{\text{cl}}(t_2)E_{\text{cl}}(t_1)|\alpha\rangle + g(\mathbf{k}_L)e^{i\omega_{\mathbf{k}_L}t_2}E_{\text{cl}}(t_1)D(\alpha)|1\rangle + g(\mathbf{k}_L)E_{\text{cl}}(t_2)e^{i\omega_{\mathbf{k}_L}t_1}D(\alpha)|1\rangle \\ &\quad + \sqrt{2}g(\mathbf{k}_L)^2e^{i\omega_L(t_1+t_2)}D(\alpha)|2\rangle - g(\mathbf{k}_L)^2e^{-i\omega_L(t_1-t_2)}|\alpha\rangle)|\{0\}_{\mathbf{k}\neq\mathbf{k}'}\rangle. \end{aligned} \quad (\text{D4})$$

In the calculations we perform in the main text, we neglect terms that are of second order with respect to  $g(\mathbf{k})$ . Therefore, under this approximation we write the action of both electric field operator components as

$$\begin{aligned} \hat{E}_{\mathbf{k}_L}(t_2)\hat{E}_{\mathbf{k}_L}(t_1)|\alpha\rangle|\{0\}_{\mathbf{k}\in\text{HH}}\rangle &\approx (E_{\text{cl}}(t_2)E_{\text{cl}}(t_1)|\alpha\rangle + g(\mathbf{k}_L)e^{i\omega_{\mathbf{k}_L}t_2}E_{\text{cl}}(t_1)D(\alpha)|1\rangle \\ &\quad + g(\mathbf{k}_L)E_{\text{cl}}(t_2)e^{i\omega_{\mathbf{k}_L}t_1}D(\alpha)|1\rangle)|\{0\}_{\mathbf{k}\neq\mathbf{k}'}\rangle. \end{aligned} \quad (\text{D5})$$

### 2. Fundamental-harmonic correlator

Here, we are going to evaluate the action of  $\hat{E}_{\mathbf{k}_L}(t_2)\hat{E}_{\mathbf{k}}(t_1)$ , where  $\mathbf{k} \neq \mathbf{k}_L$ , over the initial state of the system. We get

$$\begin{aligned} \hat{E}_{\mathbf{k}_L}(t_2)\hat{E}_{\mathbf{k}}(t_1)|\alpha\rangle|\{0\}_{\mathbf{k}\in\text{HH}}\rangle &= D(\alpha)(E_{\text{cl}}(t_2) + \hat{E}_{\mathbf{k}_L}(t_2))g(\mathbf{k})e^{i\omega_{\mathbf{k}}t_1})|1_{\mathbf{k}}\rangle|\{0\}_{\mathbf{k}'\neq\mathbf{k}}\rangle \\ &= (g(\mathbf{k})E_{\text{cl}}(t_2)e^{i\omega_{\mathbf{k}}t_1}|\alpha\rangle|1_{\mathbf{k}}\rangle + g(\mathbf{k})g(\mathbf{k}_L)e^{i(\omega_{\mathbf{k}_L}t_2+\omega_{\mathbf{k}}t_1)}D(\alpha)|1_{\mathbf{k}_L}\rangle|1_{\mathbf{k}}\rangle)|\{0\}_{\mathbf{k}'\neq\mathbf{k}_L,\mathbf{k}}\rangle, \end{aligned} \quad (\text{D6})$$

and neglecting terms of second order with respect to  $g(\mathbf{k})$ , the previous expression leads to

$$\hat{E}_{\mathbf{k}_L}(t_2)\hat{E}_{\mathbf{k}}(t_1)|\alpha\rangle|\{0\}_{\mathbf{k}\in\text{HH}}\rangle \approx g(\mathbf{k})E_{\text{cl}}(t_2)e^{i\omega_{\mathbf{k}}t_1}|\alpha\rangle|1_{\mathbf{k}}\rangle|\{0\}_{\mathbf{k}'\neq\mathbf{k}_L,\mathbf{k}}\rangle. \quad (\text{D7})$$

We note that one can easily obtain the term where the field acts over  $\mathbf{k}_L$  at  $t_1$  and over mode  $\mathbf{k}$  at  $t_2$  just by interchanging  $t_1 \leftrightarrow t_2$ .

### 3. (Different) Harmonic-harmonic correlator

Here, we are going to evaluate the action of the electric field operators defined over two different harmonic modes  $\mathbf{k} \neq \mathbf{k}'$ , that is,

$$\hat{E}_{\mathbf{k}}(t_2)\hat{E}_{\mathbf{k}'}(t_1)|\alpha\rangle|\{0\}_{\mathbf{k}\in\text{HH}}\rangle = g(\mathbf{k})g(\mathbf{k}')e^{i(\omega_{\mathbf{k}}t_2+\omega_{\mathbf{k}'}t_1)}|\alpha\rangle|1_{\mathbf{k}}\rangle|1_{\mathbf{k}'}\rangle|\{0\}_{\mathbf{k}''\neq\mathbf{k}_L,\mathbf{k},\mathbf{k}'}\rangle. \quad (\text{D8})$$

We observe that this term introduces processes where a photon of frequency  $\omega_{\mathbf{k}}$  is generated under the recombination process at time  $t_2$ , while a photon of frequency  $\omega_{\mathbf{k}'}$  is generated in the excitation process at  $t_1$  due to the vacuum fluctuations. However, since this term is proportional to a second order term in  $g(\mathbf{k})$ , we neglect it in our analysis.

### 4. (Equal) Harmonic-harmonic correlator

Lastly, we consider the scenario where the electric field operators act over the same mode  $\mathbf{k}$ . We thus get

$$\hat{E}_{\mathbf{k}}(t_2)\hat{E}_{\mathbf{k}}(t_1)|\alpha\rangle|\{0\}_{\mathbf{k}\in\text{HH}}\rangle = g(\mathbf{k})^2(\sqrt{2}e^{i\omega_{\mathbf{k}}(t_1+t_2)}|2_{\mathbf{k}}\rangle + e^{-i\omega_{\mathbf{k}}(t_2-t_1)}|0_{\mathbf{k}}\rangle)|\alpha\rangle|\{0\}_{\mathbf{k}'\neq\mathbf{k}_L,\mathbf{k}}\rangle. \quad (\text{D9})$$

In this case, we have a similar scenario to the one presented before where a photon of frequency  $\omega_{\mathbf{k}}$  is generated either at the excitation and recombination processes, so we find two photons of that frequency. On the other hand,

we also have the situation where a photon is generated in the excitation process, but it is afterwards eliminated in the recombination step. However, since these terms are proportional to  $g(\mathbf{k})^2$ , we neglect them in the main text.

Finally, after introducing these operations in the final HHG quantum state, and by further neglecting the second order terms in  $g(\mathbf{k})$ , we get

$$|\Psi_{\text{HHG}}(t)\rangle \approx \sum_{q,j,j',j''} e^{iq(j-j')} \int_{t_0}^t dt_2 \int_{\widetilde{BZ}} dp \int_{t_0}^{t_2} dt_1 e^{-\frac{i}{\hbar} \tilde{S}(q,t,t_2)} d_{j',c} \left( p - \frac{e}{c} A(t_2) \right) \\ \times e^{-\frac{i}{\hbar} S(p,t_2,t_1)} d_{j'',c}^* \left( p - \frac{e}{c} A(t_1) \right) a_{j''}^{(0)}(t_1) E_{\text{cl}}(t_2) E_{\text{cl}}(t_1) |\alpha\rangle |\{0\}_{\mathbf{k} \in \text{HH}}\rangle |w_{v,j}\rangle \quad (\text{D10})$$

$$+ \sum_{q,j,j',j''} g(\mathbf{k}_L) e^{iq(j-j')} \int_{t_0}^t dt_2 \int_{\widetilde{BZ}} dp \int_{t_0}^{t_2} dt_1 e^{-\frac{i}{\hbar} \tilde{S}(q,t,t_2)} e^{i\omega_{\mathbf{k}_L} t_2} d_{j',c} \left( p - \frac{e}{c} A(t_2) \right) \\ \times e^{-\frac{i}{\hbar} S(p,t_2,t_1)} E_{\text{cl}}(t_1) d_{j'',c}^* \left( p - \frac{e}{c} A(t_1) \right) a_{j''}^{(0)}(t_1) D(\alpha) |1_{\mathbf{k}_L}\rangle |\{0\}_{\mathbf{k} \in \text{HH}}\rangle |w_{v,j}\rangle \quad (\text{D11})$$

$$+ \sum_{q,j,j',j''} g(\mathbf{k}_L) e^{iq(j-j')} \int_{t_0}^t dt_2 \int_{\widetilde{BZ}} dp \int_{t_0}^{t_2} dt_1 e^{-\frac{i}{\hbar} \tilde{S}(q,t,t_2)} E_{\text{cl}}(t_2) d_{j',c} \left( p - \frac{e}{c} A(t_2) \right) \\ \times e^{-\frac{i}{\hbar} S(p,t_2,t_1)} d_{j'',c}^* e^{i\omega_{\mathbf{k}_L} t_1} \left( p - \frac{e}{c} A(t_1) \right) a_{j''}^{(0)}(t_1) D(\alpha) |1_{\mathbf{k}_L}\rangle |\{0\}_{\mathbf{k} \in \text{HH}}\rangle |w_{v,j}\rangle \quad (\text{D12})$$

$$+ \sum_{\mathbf{k},q,j,j',j''} g(\mathbf{k}) e^{iq(j-j')} \int_{t_0}^t dt_2 \int_{\widetilde{BZ}} dp \int_{t_0}^{t_2} dt_1 e^{-\frac{i}{\hbar} \tilde{S}(q,t,t_2)} e^{i\omega_{\mathbf{k}} t_2} d_{j',c} \left( p - \frac{e}{c} A(t_2) \right) \\ \times e^{-\frac{i}{\hbar} S(p,t_2,t_1)} E_{\text{cl}}(t_1) d_{j'',c}^* \left( p - \frac{e}{c} A(t_1) \right) a_{j''}^{(0)}(t_1) |\alpha\rangle |1_{\mathbf{k}}\rangle |\{0\}_{\mathbf{k}' \neq \mathbf{k}}\rangle |w_{v,j}\rangle \quad (\text{D13})$$

$$+ \sum_{\mathbf{k},q,j,j',j''} g(\mathbf{k}) e^{iq(j-j')} \int_{t_0}^t dt_2 \int_{\widetilde{BZ}} dp \int_{t_0}^{t_2} dt_1 e^{-\frac{i}{\hbar} \tilde{S}(q,t,t_2)} E_{\text{cl}}(t_2) d_{j',c} \left( p - \frac{e}{c} A(t_2) \right) \\ \times e^{-\frac{i}{\hbar} S(p,t_2,t_1)} d_{j'',c}^* e^{i\omega_{\mathbf{k}} t_1} \left( p - \frac{e}{c} A(t_1) \right) a_{j''}^{(0)}(t_1) |\alpha\rangle |1_{\mathbf{k}}\rangle |\{0\}_{\mathbf{k}' \neq \mathbf{k}}\rangle |w_{v,j}\rangle. \quad (\text{D14})$$

### E. Step-by-step derivation of the *conditioned to HHG* state

As mentioned in the main text, non-classical states of light can be obtained after high-harmonic generation processes by means of an heralding scheme. In this set-up, a correlation measurement between the harmonic and part of the fundamental mode is carried out. Specifically, we look at events where the generation of photons at high frequencies relies on a perturbation of the fundamental mode. From a mathematical point of view, we characterize this operation via the projector

$$\hat{P}_{\text{HHG}} = \mathbb{1} - |\alpha\rangle\langle\alpha| \bigotimes_{\mathbf{k} \in \text{HH}} |0_{\mathbf{k}}\rangle\langle 0_{\mathbf{k}}|, \quad (\text{E1})$$

which we refer to as *conditioning to HHG* operation. In this expression, we are looking at all those events where both the fundamental and the harmonic modes are not found in the original state in which they initially were when the dynamics started.

We now apply the projector in Eq. (E1) to the state obtained at the end of the previous section

$$|\Psi_{\text{cond}}(t)\rangle = \hat{P}_{\text{HHG}} |\Psi(t)\rangle \approx |\Psi_{\text{HHG}}(t)\rangle - \langle \alpha, \{0\}_{\mathbf{k} \in \text{HH}} | \Psi_{\text{HHG}}(t) \rangle |\alpha\rangle |\{0\}_{\mathbf{k} \in \text{HH}}\rangle, \quad (\text{E2})$$

where we neglect the terms arising from  $|\Psi'_{\text{ion}}(t)\rangle$ , as the only terms that contribute are those where an electron is generated at the ionization time due to vacuum fluctuations, and their effect is negligible when looking at the HHG contributions.

When performing this conditioning operation, we observe that the term in Eq. (D10) vanishes because of the subtraction appearing in Eq. (E1), while the second term of this conditioning operation eliminates all the terms from Eq. (D11) to Eq. (D14). In particular, the ones in Eqs. (D11) and (D12) are eliminated because

$$\langle \alpha | D(\alpha) | 1_{\mathbf{k}_L} \rangle = \langle 0_{\mathbf{k}_L} | D^\dagger(\alpha) D(\alpha) | 1_{\mathbf{k}_L} \rangle = \langle 0_{\mathbf{k}_L} | 1_{\mathbf{k}_L} \rangle = 0. \quad (\text{E3})$$

Thus, the final state we get right after the conditioning operation is given by

$$|\Psi_{\text{cond}}(t)\rangle = \sum_j \mathcal{P}_{\text{total}}(j, 1_{\mathbf{k}_L}, t) D(\alpha) |1_{\mathbf{k}_L}\rangle |\{0\}_{\mathbf{k} \in \text{HH}}\rangle |w_{v,j}\rangle + \sum_{j,\mathbf{k}} \mathcal{P}_{\text{total}}(j, 1_{\mathbf{k}}, t) |\alpha\rangle |1_{\mathbf{k}}\rangle |\{0\}_{\mathbf{k}' \neq \mathbf{k}}\rangle |w_{v,j}\rangle, \quad (\text{E4})$$

where  $\mathcal{P}_{\text{total}}(j, 1_{\mathbf{k}}, t) = \sum_{i=1,2} \mathcal{P}^{(i)}(j, 1_{\mathbf{k}}, t)$ , with  $\mathcal{P}^{(i)}(j, 1_{\mathbf{k}}, t)$  are defined in Eqs. (37) and (38) for  $i = 1$  and  $i = 2$ , respectively.

### F. Quantities computed when measuring the fundamental mode

In this section, we develop the expression of the entanglement measures and fidelity quantities we use in the main text when measuring the fundamental mode of our HHG state, i.e., for the state

$$|\Psi_{\text{cond}}^{(\text{XUV})}(t)\rangle = \langle \alpha | \Psi_{\text{cond}}(t) \rangle = \sum_{j,\mathbf{k}} \mathcal{P}_{\text{total}}(j, 1_{\mathbf{k}}, t) |1_{\mathbf{k}}\rangle |\{0\}_{\mathbf{k}' \neq \mathbf{k}}\rangle |w_{v,j}\rangle. \quad (\text{F1})$$

As a brief summary, we used the entropy of entanglement as an entanglement measure for the light-matter entanglement characterization; we studied how close the conditioned to HHG state, after measuring the fundamental modes, is to a  $W$  state of length  $M$ ; finally, we studied the entanglement between the different field modes by means of the logarithmic negativity.

#### 1. Entropy of entanglement

The entropy of entanglement is an entanglement measure defined for pure states as

$$S(\rho) := -\text{tr}(\rho \log \rho), \quad (\text{F2})$$

where  $\rho$  is the reduced density matrix with respect to one of the subsystems. In our case, the full density matrix of our system can be written as

$$\rho_{\text{full}} = \sum_{j,j'} |w_{v,j}\rangle \langle w_{v,j'}| \otimes |\Lambda_j\rangle \langle \Lambda_{j'}|, \quad (\text{F3})$$

where we have defined

$$|\Lambda_j\rangle = \sum_{\mathbf{k}} \mathcal{P}_{\text{total}}(j, 1_{\mathbf{k}}, t) |1_{\mathbf{k}}\rangle |\{0\}_{\mathbf{k}' \neq \mathbf{k}}\rangle, \quad (\text{F4})$$

and therefore the reduced density matrix with respect to the quantum optical degrees of freedom can be written as

$$\rho = \sum_{j,j'} \langle \Lambda_{j'} | \Lambda_j \rangle |w_{v,j}\rangle \langle w_{v,j'}| \quad (\text{F5})$$

In principle, there is no difference on what subsystem is traced out: both reduced density matrices lead to the same result. However, in our case we restrict our study to three Wannier sites  $j \in \{-1, 0, 1\}$ , while we let the harmonic modes to populate a continuum of modes. Therefore, this choice is more practical from the numerical computations since the reduced density matrix with respect to the field modes is a  $3 \times 3$  matrix that can be easily implemented numerically, which we did in Python (the codes employed in the numerical analysis can be found in Ref. [99]). Thus, by using the `scipy.linalg` package [100] which has functions that allow to compute the logarithm of a matrix, the entropy of entanglement can be easily and efficiently evaluated. In fact, this operation takes on the order of 1 second in the employed machine, a MacBook Air M1 (2020) with 8 CPU cores.

#### 2. Fidelity with respect to a $W$ state of length $M$

Here, we are going to derive the expressions presented in the main text regarding the fidelity. This quantity provides a measure of *closeness* between two distinct quantum states. It is formally defined as

$$F(\sigma, \rho) := \left[ \text{tr} \left( \sqrt{\sqrt{\sigma} \rho \sqrt{\sigma}} \right) \right]^2, \quad (\text{F6})$$

and it is symmetric with respect to a swap between the states, i.e.,  $F(\sigma, \rho) = F(\rho, \sigma)$  [83]. In our case, one of the states would correspond to the one we want to study, while the other is the state we want to compare against with, which in our case is the  $W$  state of length  $M$  and that we defined as

$$|W_M\rangle = \frac{1}{\sqrt{M}} \sum_n |1_n\rangle |\{0\}_{n' \neq n}\rangle. \quad (\text{F7})$$

Since this state is pure, we select it for convenience to be  $\sigma$  in Eq. (F6), such that we can write

$$\begin{aligned} F(|W_M\rangle, \rho) &= \left[ \text{tr} \left( \sqrt{\sqrt{|W_M\rangle\langle W_M|} \rho \sqrt{|W_M\rangle\langle W_M|}} \right) \right]^2 = \left[ \text{tr} \left( \sqrt{\langle W_M|\rho|W_M\rangle} |W_M\rangle\langle W_M| \right) \right]^2 \\ &= \langle W_M|\rho|W_M\rangle, \end{aligned} \quad (\text{F8})$$

and we now proceed to consider different candidates for  $\rho$ . One of them would be the state in Eq. (F1) when projecting onto a particular Wannier state  $|w_{v,j}\rangle$ , i.e.

$$\left| \Psi_j^{(\text{XUV})}(t) \right\rangle = \left\langle w_{v,j} \left| \Psi_{\text{cond}}^{(\text{XUV})}(t) \right\rangle \right\rangle = \sum_{j,\mathbf{k}} \mathcal{P}_{\text{total}}(j, 1_{\mathbf{k}}, t) |1_{\mathbf{k}}\rangle |\{0\}_{\mathbf{k}' \neq \mathbf{k}}\rangle, \quad (\text{F9})$$

for which the fidelity adopts the following expression

$$F(|W_M\rangle, |\Psi_j^{(\text{XUV})}(t)\rangle) = \frac{1}{M} \sum_{\mathbf{k}, \mathbf{k}'} \mathcal{P}_{\text{total}}(j, 1_{\mathbf{k}}, t) \mathcal{P}_{\text{total}}^*(j, 1_{\mathbf{k}'}, t) = \frac{1}{M} \left| \sum_{\mathbf{k}} \mathcal{P}_{\text{total}}(j, 1_{\mathbf{k}}, t) \right|^2. \quad (\text{F10})$$

On the other hand, from a more realistic experimental perspective, one could trace out the electronic degrees of freedom in Eq. (F1) to get

$$\rho^{(\text{XUV})} = \sum_{j, \mathbf{k}, \mathbf{k}'} \mathcal{P}_{\text{total}}(j, 1_{\mathbf{k}}, t) \mathcal{P}_{\text{total}}^*(j, 1_{\mathbf{k}'}, t) |1_{\mathbf{k}}, \{0\}_{\tilde{\mathbf{k}} \neq \mathbf{k}}\rangle \langle 1_{\mathbf{k}'}, \{0\}_{\tilde{\mathbf{k}}' \neq \mathbf{k}'}|, \quad (\text{F11})$$

such that in this case the fidelity reads

$$F(|W_M\rangle, \rho^{(\text{XUV})}) = \frac{1}{M} \sum_{j, \mathbf{k}, \mathbf{k}'} \mathcal{P}_{\text{total}}(j, 1_{\mathbf{k}}, t) \mathcal{P}_{\text{total}}^*(j, 1_{\mathbf{k}'}, t). \quad (\text{F12})$$

### 3. Logarithmic negativity

In order to study the entanglement between the field modes, we first trace out the electronic degrees of freedom. One could in principle project over a given Wannier state, but instead we restrict ourselves to the realistic experimental scenario where we cannot distinguish in which state has the electron recombined in. Thus, we are left with the mixed state presented in Eq. (F1). In principle, the entanglement characterization of mixed states is a problem that has not a universal solution: there are some entanglement measures that are able to witness entanglement under specific scenarios. Furthermore, we have an extra complication, and is that we have a multipartite state. Thus, instead of dealing with a multipartite scenario, we instead by split our state in two parts  $A$  and  $B$ , such that some of the frequencies belong to subsystem  $A$ , while others belong to subsystem  $B$ . Thus, in this bipartite scenario, we can rewrite our state as

$$\begin{aligned} \rho_{AB} &= \sum_j \left[ |\Lambda_{A,j}\rangle\langle\Lambda_{A,j}| \otimes |\{0\}_B\rangle\langle\{0\}_B| + |\{0\}_A\rangle\langle\{0\}_A| \otimes |\Lambda_{B,j}\rangle\langle\Lambda_{B,j}| \right. \\ &\quad \left. + |\Lambda_{A,j}\rangle\langle 0_{A,j}| \otimes |\{0\}_B\rangle\langle\Lambda_{B,j}| + |0_{A,j}\rangle\langle\Lambda_{A,j}| \otimes |\Lambda_{B,j}\rangle\langle\{0\}_B| \right], \end{aligned} \quad (\text{F13})$$

where we have defined

$$|\Lambda_{A,j}\rangle = \sum_{\mathbf{k} \in O_A} \mathcal{P}_{\text{total}}(j, 1_{\mathbf{k}}, t) |1_{\mathbf{k}}\rangle |\{0\}_{\mathbf{k}' \neq \mathbf{k}}\rangle, \quad (\text{F14})$$

with  $O_A$  the set of frequencies belonging to subsystem  $A$ . A similar definition, substituting  $A$  by  $B$ , follows for subsystem  $B$ .

In this scenario, the logarithmic negativity is an appropriate entanglement measure, and is defined as

$$E_N(\rho) := \log_2(2N(\rho_{AB}) + 1), \quad (\text{F15})$$

where  $N(\rho_{AB})$  is the negativity of the measured state, which is defined as the sum over all negative eigenvalues of the partial transpose with respect to one of the subsystems of  $\rho_{AB}$ . If we choose subsystem  $A$  (although subsystem  $B$  can be chosen as well leading to the same results), the partial transposed state  $\rho_{AB}^{T_A}$  reads

$$\begin{aligned} \rho_{AB}^{T_A} = \sum_j & \left[ \left( |\Lambda_{A,j}\rangle\langle\Lambda_{A,j}| \right)^{T_A} \otimes |\{0\}_B\rangle\langle\{0\}_B| + |\{0\}_A\rangle\langle\{0\}_A| \otimes |\Lambda_{B,j}\rangle\langle\Lambda_{B,j}| \right. \\ & \left. + \left( |\Lambda_{A,j}\rangle\langle\Lambda_{A,j}| \right)^{T_A} \otimes |\{0\}_B\rangle\langle\Lambda_{B,j}| + \left( |\Lambda_{A,j}\rangle\langle\Lambda_{A,j}| \right)^{T_A} \otimes |\Lambda_{B,j}\rangle\langle\{0\}_B| \right]. \end{aligned} \quad (\text{F16})$$

This operation has been numerically implemented in Python, and the corresponding codes can be found in Ref. [99]. From here, after diagonalizing the partial transposed state, we may find a set of negative eigenvalues  $\{\lambda_j^{(-)}\}$ . Then, the negativity can be computed as

$$N(\rho_{AB}) = \left| \sum_j \lambda_j^{(-)} \right|^2, \quad (\text{F17})$$

and which introduced in the entropy of entanglement definition leads to

$$E_N(\rho_{AB}) = \log_2 \left( 2 \left| \sum_j \lambda_j^{(-)} \right|^2 + 1 \right). \quad (\text{F18})$$

Thus, if there are no negative eigenvalues, we get  $E_N(\rho_{AB}) = 0$ . However, from this result we cannot conclude that the state is entangled or not, i.e., there might be other entanglement measures that are non-vanishing for states that have a vanishing entropy of entanglement.

#### G. Decoherence effects on the harmonic emission

One of the main advantages of the Bloch-Bloch representation with respect to the Wannier-Bloch approach we introduce here, is that the former is a density matrix approach, while in the latter we have to solve the Schrödinger equation for a single-electron. Thus, the introduction of decoherence effects may become a ponderous task in the Wannier-Bloch approach, while in the Bloch-Bloch approach can be introduced naturally at the level of the semiconductor Bloch equations, as shown for example in Eq. (24) of Ref. [101], by means of a relaxation time  $T_2$ . Thus, in order to understand how decoherence effects affect the harmonic emission, we consider here (and only here) a Bloch-Bloch approach.

In Fig. 10, we show with continuous (dashed) curves the contributions of interband and intraband dynamics to the harmonic spectrum when decoherence effects are (not) taken into account. These are introduced by means of a finite relaxation time  $T_2 = 5.5$  fs. We observe that, when decoherence effects enter into the dynamics, the harmonic plateau gets reduced. This is an expected feature, as the electron has another route, via relaxation, for returning to the valence band and which does not involve a recombination process. Furthermore, we see that intraband and interband contributions become comparable for low harmonic orders. However, and regarding the quantum optical observables we study in the main text such as the Wigner function after the conditioning operation, we do not expect very important modifications to show up. This is because the kind of decoherence that appears here only affects the electronic degrees of freedom, and only affect the quantum optical degrees of freedom via the modifications in the harmonic plateau. Thus, a reduction of the overall intensity of the harmonics implies a lower chance of performing the *conditioning to HHG* operation successfully. Nevertheless, when the latter takes place, the negativities in the Wigner function could be potentially observed if the harmonic range used is the appropriate one.

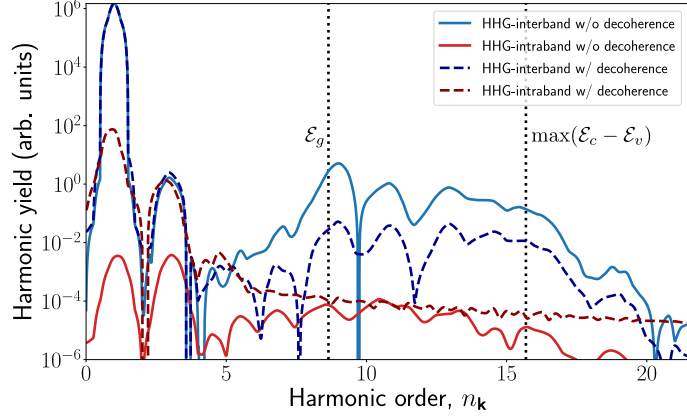


FIG. 10. Harmonic spectrum contribution of interband (blue curves) and intraband (red curves) dynamics depending on importance of decoherence effects. The continuous curves correspond to the case where decoherence is not introduced ( $T_2 \rightarrow \infty$ ), while in the dashed curves we have introduced a finite relaxation time  $T_2 = 227.37$  a.u., i.e., 5.5 fs. The solid system is ZnO and the laser field has polarization along the  $\Gamma - A$  direction, with 4 cycles of duration, a sinusoidal-squared envelope, central wavelength  $\lambda_L = 3.25 \mu\text{m}$ , and peak intensity  $I_0 = 5 \times 10^{11} \text{ W/cm}^2$ . This spectrum has been computed using a Bloch-Bloch approach. Note that, independently of the theory that is used, the harmonic spectrum is in very good agreement with the one shown in Fig. 4 (b).